

JGR Solid Earth

RESEARCH ARTICLE

10.1029/2023JB026759

Special Section:

Solid Earth Geophysics as a means to address issues of global change

Key Points:

- Seismic velocity at short periods are influenced by the hydrologic cycle and the amount of water within aquifers
- A simple linear model can predict the evolution of seismic wave velocity from precipitation
- We show that Global Positioning System measurement, hydraulic heads and velocity variations are complementary tools to monitor aquifers

Supporting Information:

Supporting Information may be found in the online version of this article.

Correspondence to:

E. Delouche,
estelle.delouche@univ-grenoble-alpes.fr

Citation:

Delouche, E., & Stehly, L. (2023). Seasonal seismic velocity variations measured using seismic noise autocorrelations to monitor the dynamic of aquifers in Greece. *Journal of Geophysical Research: Solid Earth*, 128, e2023JB026759. <https://doi.org/10.1029/2023JB026759>

Received 17 MAR 2023

Accepted 13 NOV 2023

Author Contributions:

Funding acquisition: L. Stehly
Investigation: E. Delouche
Methodology: E. Delouche
Supervision: L. Stehly
Writing – original draft: E. Delouche

© 2023. The Authors.

This is an open access article under the terms of the Creative Commons Attribution-NonCommercial-NoDerivs License, which permits use and distribution in any medium, provided the original work is properly cited, the use is non-commercial and no modifications or adaptations are made.

Seasonal Seismic Velocity Variations Measured Using Seismic Noise Autocorrelations to Monitor the Dynamic of Aquifers in Greece

E. Delouche¹  and L. Stehly¹

¹Univ. Grenoble Alpes, Univ. Savoie Mont Blanc, CNRS, IRD, UGE, ISTerre, Grenoble, France

Abstract Monitoring groundwater levels in aquifers is crucial for water resources management on a global scale. In Greece, water stress is particularly high due to the expansion of agricultural land, urbanization and tourism, leading to aquifer over-exploitation. In this study, we investigate the possibility of monitoring groundwater reservoirs from seismic velocity changes ($\delta v/v$) measured using noise autocorrelations. The results obtained at short periods (0.5–3 s) indicate that in several regions, seismic wave velocity varies according to an annual cycle mainly controlled by aquifer loading and discharge. We also predict seismic velocity variations from a simple model using precipitation records. In addition, this model provides a proxy for the characteristic time of aquifer discharge rate and allows us to distinguish shallow alluvial aquifers (~100 m) from deep karst systems (~1 km). Finally, we study the effect of water pumping from groundwater reservoirs. To that end, we combine Global Positioning System (GPS), hydraulic heads and velocity variations measurement. The results indicate that confined and unconfined aquifers respond differently. While for unconfined aquifers, pumping water implies an uplift of the surface, we show that for confined aquifers a subsidence occurs, due to the consolidation of the sediments at depth. Being an in-situ and volumetric measurement, the $\delta v/v$ is primarily sensitive to the amount of water stored in the entire aquifer system, whereas GPS measurements provide the deformation at the surface induced by both deep sediment compaction and water level variations. These observations show that GPS, hydraulic head, and $\delta v/v$ are complementary tools to monitor aquifers.

Plain Language Summary Monitoring the evolution of groundwater resources is an issue for the twenty-first century. The expansion of agricultural land, urbanization and tourism are depleting aquifers. In this study, we propose to monitor groundwater reservoirs from the evolution of seismic wave velocity. The results obtained in Greece indicate that in several regions, the seismic wave velocity varies according to an annual cycle mainly controlled by aquifer loading and discharge. Hence by using continuous seismic noise records it is possible to track the evolution of aquifers over time and to distinguish shallow (~100 m) from deep aquifers (~1 km). Finally, we study the effect of water pumping from groundwater reservoirs. To that end, we combine Global Positioning System surface deformation measurements with seismic velocity variations. The results indicate that confined and unconfined aquifers respond differently. While for unconfined aquifers, pumping water implies an uplift of the surface, we show that for confined aquifers a subsidence occurs, due to the consolidation of the sediments at depth. While for unconfined aquifers, these surface variations are transient, the drainage of confined aquifers due to pumping is permanent.

1. Introduction

Worldwide, aquifers are essential groundwater reservoirs for agriculture, residential and industrial activities. In the Mediterranean basin, aquifers are the main exploitable resource for drinking water supply and agriculture. The increasing demands of the last decades conduct to excessive exploitation of groundwater resources. This may lead either to the depletion of aquifers, or to their contamination by seawater and agricultural pollutants. Currently, Greece is ranked 26th in the world among the countries most affected by water stress (Heggie, 2020). Its freshwater supply depends mainly on groundwater, with over 300,000 wells throughout the country (Daskalaki & Voudouris, 2008). Intense urbanization, the development of tourism, and the expansion of agricultural land attend to intensive exploitation of water resources, especially from April to October, which are the most critical months. Currently, agriculture represents the main demand for water and covers about 86% of the total water consumption (Daskalaki & Voudouris, 2008; Mimikou, 2005). Thus, studying the temporal monitoring of these resources has become essential from a societal and an ecological perspective.

Writing – review & editing: E. Delouche, L. Stehly

Several geophysical tools allow to characterize the state and dynamics of aquifers. Direct measurements of the hydraulic heads provide in situ measurements of groundwater levels. These measurements are punctual in space and cannot provide a global view of the dynamics of large aquifer systems. Global Positioning System (GPS) and interferometric synthetic aperture radar (InSAR) measure surface deformation with high temporal and spatial resolution, but cannot detect processes that do not affect the surface nor constrain the depth of perturbations (Amos et al., 2014; Argus et al., 2014; Bawden et al., 2001; Borsa et al., 2014; Chen & Liu, 2016; Ji & Herring, 2012; Lanari et al., 2004; Riel et al., 2018). Gravimetric measurements from satellites such as Gravity Recovery and Climate Experiment (GRACE), can be used to track changes in the amount of water stored in aquifers on a large scale but with limited spatial (hundred kilometers) and temporal (monthly) resolution (Frappart & Ramillien, 2018; Rodell et al., 2009).

Recently, the use of seismic noise correlations to monitor seismic velocity ($\delta v/v$) in time and space has shown to be a promising tool for monitoring aquifer evolution (Almagro Vidal et al., 2021; Barajas et al., 2021; Clements & Denolle, 2018; Mao et al., 2022), and more generally to detect velocity changes in the crust (Brenguier et al., 2008; Wegler & Sens-Schönfelder, 2007). This method consists in repeatedly extracting the Green's function of the medium between pairs of receivers in (ideally) a dense array by correlating the ambient noise records. Seismic wave velocity change within the medium can be tracked by analyzing the coda part of the reconstructed Green's function. By using noise correlations filtered in different period bands and/or by analyzing different coda time windows, different depths can be monitored ranging from a few meters (Hillers et al., 2015; Sens-Schönfelder & Wegler, 2006) to the middle and lower crust (Froment et al., 2013; Obermann et al., 2014; Poli et al., 2020; Rivet et al., 2013; Wang et al., 2019).

The evolution of seismic wave velocity reflects changes in the mechanical properties of the crust that can be induced by changes in the stress field, fluid content, or by rock damage for instance. Thus, a variety of processes can induce velocity changes, such as long-term post-seismic relaxation following earthquakes and deep creep in fault zone (Brenguier et al., 2008; Froment et al., 2013; Hillers et al., 2019; Zaccarelli et al., 2011), slow slip events in subduction zone (Rivet et al., 2011), and volcanic eruptions (Brenguier et al., 2008, 2011; Obermann et al., 2013; Wegler & Sens-Schönfelder, 2007). However, the evolution of seismic wave velocity in the crust is not only related to tectonic processes and can also result from environmental changes such as precipitation (Hillers et al., 2014; Meier et al., 2010; Sens-Schönfelder & Wegler, 2006; Tsai, 2011), thermoelastic stresses (Hillers et al., 2015; Meier et al., 2010), and even atmospheric pressure (Silver et al., 2007).

Monitoring aquifers using seismic noise correlations is particularly interesting since seismic waves provide an in situ and volumetric measurement of the elastic properties of the medium, and are sensitive to changes in pore pressure, porosity, saturation, and density, as well as the presence of microcracks. Therefore, $\delta v/v$ measurements are complementary to other geophysical tools such as GPS/INSAR which measure surface deformation, and hydraulic head measurements which provide spatially sparse measurements of water level. A change in hydraulic loading affects seismic velocities primarily through (a) the elastic response of the crust due to the change in water-loading pressure which can also subside the surface (Faunt et al., 2016; Galloway et al., 1999) and (b) the poroelastic response induced by recharge of the internal porous soil structure of the aquifer (Barajas et al., 2021; Bettinelli et al., 2008; Galloway & Burbey, 2011; King et al., 2007; Overacker et al., 2022).

Silverii et al. (2016) have used the GPS data in the Apennines to show that the multiyear hydrologic cycle associated with the recharge and discharge phase of the karst aquifer modulates extensional deformation by 3 mm/year. The vertical component exhibits seasonal and multiyear signals reflecting the elastic response of the lithosphere to variations in surface water loads. While the horizontal motions record an expansion/contraction poroelastic effect in the aquifer (Amoruso et al., 2014; Barajas et al., 2021; Chaussard et al., 2014; Ojha et al., 2019; Silverii et al., 2016). Finally, this hydrologic forcing associated with karst aquifer recharge induces measurable surface deformation up to 50 nanostrain per year (D'Agostino, 2014).

If Greece is one of the countries of the Mediterranean basin to be particularly affected by water stress, it is also one of the most seismic areas in Europe with more than 15,000 earthquakes detected each year (from Institute of Geodynamics, NOA (Ktenidou & Evangelidis, 2023)). Earthquakes occur on fault systems due to long-term stress accumulation and transient triggering mechanisms. However, our current understanding of earthquake preparation, nucleation, and consequences on crustal properties is still limited. Using noise correlation to monitor the spatio-temporal evolution of crustal mechanical properties could also provide new insight into the seismic cycle. To determine seismic wave velocity variations specifically related to tectonic processes, it is necessary to

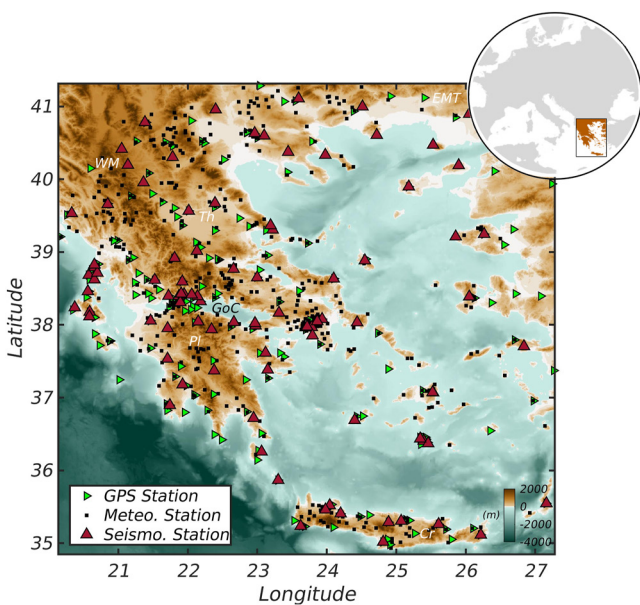


Figure 1. Distribution of the seismological stations (red triangles), meteorological stations (black squares), and GPS stations (green triangles) in Greece. Mention: Gulf of Corinth (GoC); Peloponnese (Pl); Crete (Cr); Thessaly region (Th); East Macedonia and Thrace (EMT) and western Macedonia(WM).

publicly available permanent broadband seismic stations in Greece from January 2010 to March 2022. This includes the data of 90 stations as shown on Figure 1. The stations used are distributed across Greece with an average inter-station distance of 40 km, with a higher density around the Gulf of Corinth (GoC) thanks to the dense Corinth Rift Laboratory Network. This makes this data set particularly well suited to study the evolution of the seismic wave velocity with a decent spatial and temporal resolution.

2.2. Data Processing and Noise Correlations

We processed the noise records in the following way: first, the data were corrected from the instrumental response and decimated to 5 Hz. To downweight the contribution of energetic signals, such as glitches, earthquakes, or oceanic storms, the amplitude of the records is normalized in the time domain, by dividing them by their envelope in the 1–3 s period band. This is similar to the “comb-filter” used by Nouibat et al. (2022) and Soergel et al. (2020).

For each station, we compute the auto-correlation of the normalized vertical records using a sliding window of 4 hr. Instead of analyzing these 4 hr correlations, we consider 60-day-stacked correlations to increase the signal-to-noise ratio. The n -day-stacked correlations were obtained by stacking the 4 hr correlations with a sliding window of n days that is shifted by 5 days. In the following, we consider that these auto-correlations are an approximation of the Green's function between a source and a receiver that are both located at the station. Therefore, the use of autocorrelations therefore makes it possible to measure velocity changes in the vicinity of each station that are easier to interpret than $\delta v/v$ obtained from cross-correlations which are sensitive to a larger area.

2.3. Computing $\delta v/v$ Using the Stretching Method

Our goal is to measure the temporal evolution of the seismic wave velocity across Greece using noise auto-correlations. Measurements are made in the 1–3 s period band to get a global view of shallow velocity

be able to correct the $\delta v/v$ measurements for the contribution of environmental factors and the hydrologic cycle. The use of noise correlations to monitor aquifers is therefore useful for studying the hydrologic cycle in itself and indirectly for identifying changes in the crust related to tectonic processes (Barajas et al., 2021).

In this study, we assess the possibility of using seismic noise correlations to characterize the evolution of aquifers across Greece where two types of aquifers coexist: karst aquifers, which are mainly found in carbonate rocks that cover about 35% of the country; and aquifers located in alluvial layers dating from the Neogene and Quaternary. To that end, we use all publicly available broadband seismic stations to track changes in seismic velocity in the 1–3 s period band. The manuscript is organized as follows: Section 2 describes the data set used and how seismic velocity variations are measured from noise correlation. We show in Section 3, that in specific regions, the seismic velocity changes with the season. Using 495 weather stations, we show in Section 4 that at some sites, the observed $\delta v/v$ can be predicted from precipitation. Assuming a simple linear reservoir model, this allows us to estimate the discharge rate at each site. Finally, we specifically study how water pumping for agriculture and industry induces seismic wave velocity variations in two cases: an unconfined aquifer in Crete and a confined aquifer in Thessaly.

2. Data Processing

2.1. Seismological Stations

Our aim is to measure relative seismic velocity changes ($\delta v/v$) in the upper crust in Greece. To that end, we use continuous vertical noise records at all

publicly available permanent broadband seismic stations in Greece from January 2010 to March 2022. This

includes the data of 90 stations as shown on Figure 1. The stations used are distributed across Greece with an

average inter-station distance of 40 km, with a higher density around the Gulf of Corinth (GoC) thanks to the

dense Corinth Rift Laboratory Network. This makes this data set particularly well suited to study the evolution of

the seismic wave velocity with a decent spatial and temporal resolution.

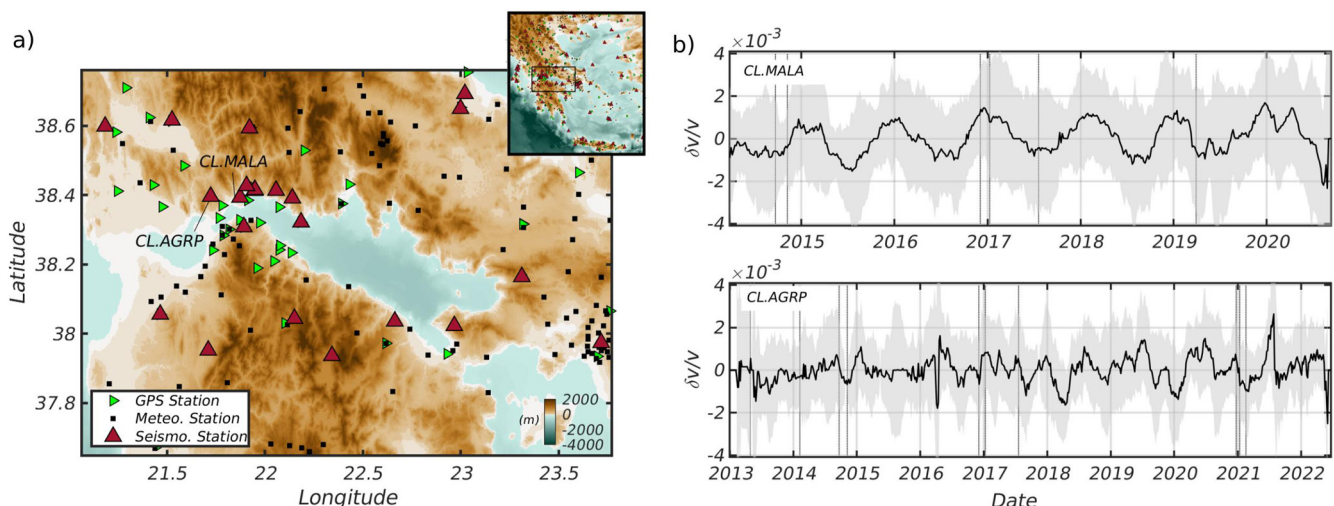


Figure 2. (a) Map of the Gulf of Corinth showing the location of the seismological stations MALA and AGRP. (b) Evolution of the seismic velocities $\delta v/v$ in the 1–3 s period band obtained with a sliding window of 60 days (black solid line) and the corresponding errorbars (gray shaded area) at two stations separated by 13 km: MALA (upper panel) and AGRP (lower panel). The vertical dashed lines represent the seismic events of $M > 4.5$ in a radius of 50 km. At MALA the seismic velocity exhibits clear seasonal variations having an amplitude of $\pm 0.1\%$. These seasonal variations are not observed at AGRP station.

variations, and in narrower bands (0.5–1 s, 1–2 s, 2–3 s) to assess the depth of changes detected more precisely. We use specifically coda waves in the 15–55 s time window since coda waves are more sensitive to weak changes in the medium than direct waves (Froment et al., 2010).

In order to get the highest quality measurements we choose to use the stretching method (Lobkis & Weaver, 2003; Sens-Schönfelder & Wegler, 2006); which is less sensitive to noisy data than the doublet method (Hadzioannou et al., 2011). For each station, we first define a reference auto-correlation which is the correlation averaged for the whole period 2010–2022. We then track medium changes by comparing each 60-day auto-correlation with the reference auto-correlation.

Assuming a spatially homogeneous change in the medium velocity, the relative velocity change $\delta v/v$ at a given date is the stretching coefficient $\epsilon = \delta v/v$ that has to be applied to the auto-correlation corresponding to this date to maximize its similarity with the reference auto-correlation. This stretching coefficient is determined by a grid search. Ideally, the correlation coefficient between the current and the reference auto-correlation should be close equal to one. A value less than one indicates a change in the noise sources or in the scattering properties of the medium or that the velocity change is not spatially homogeneous (Hadzioannou et al., 2011).

Weaver et al. (2011) have shown that when the stretching method is used to infer velocity changes, the root mean square (RMS) of the errors of the estimate of the relative velocity change between a reference correlation and a N -days (auto)correlations is given by:

$$rms(\epsilon) = \frac{\sqrt{1-X^2}}{2X} \sqrt{\frac{6\sqrt{\frac{\pi}{2}}T}{\omega_c^2(t_2^3-t_1^3)}} \quad (1)$$

where X is the correlation coefficient between the reference and the N -days correlation, T is the inverse of the frequency bandwidth, ω_c is the central pulsation, t_1 and t_2 are begin and end time of the coda window analyzed. When using a sliding window of N days, the correlation coefficients X between the N -days auto-correlations and the reference is expected to increase with N and the RMS of the $\delta v/v$ measurements to decrease. Similarly the RMS decreases when the length of the coda window used $t_2 - t_1$ increases. Conversely, if the velocity change is not homogeneous, as we have assumed, the correlation coefficient X will be lower, resulting in a higher rms value.

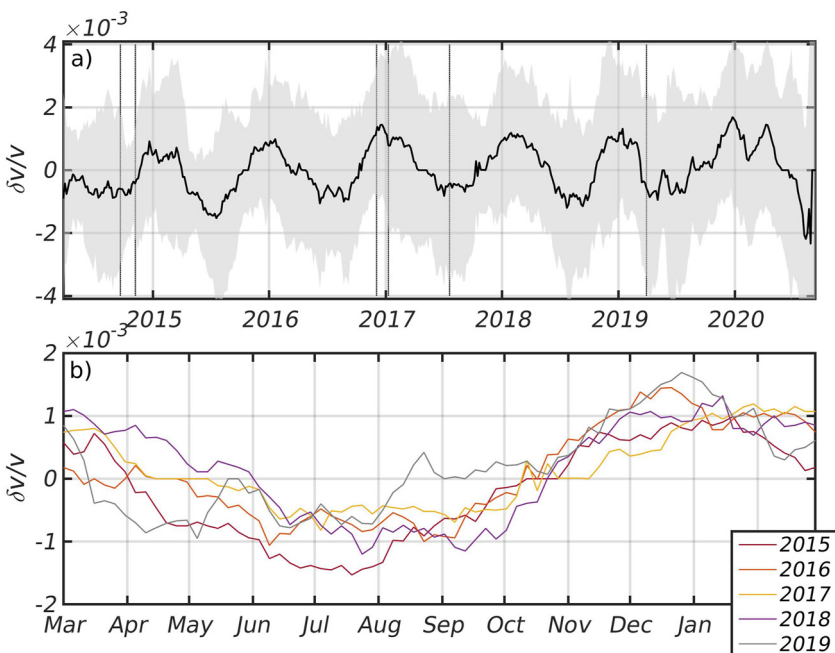


Figure 3. (a) $\delta v/v$ computed at the station MALA in the 1–3 s period band with a sliding window of 60 days (black solid line) and the error bars of the measurements (gray shaded area). The dashed lines represent seismic events of $M_w > 4.5$ that have occurred in a radius of 50 km around MALA. Seasonal variations are clearly visible with an amplitude of $\pm 0.1\%$, the velocity being maximum in winter and minimum in summer. (b) Annual $\delta v/v$ from 1 March to 28 February measured at MALA from 2015 to 2019. We note that each year the seismic velocity exhibits similar seasonal variations.

2.4. Example of $\delta v/v$ Measurements in the Gulf of Corinth

Figure 2 presents the temporal evolution of the coda wave velocity measured at two stations MALA and AGRP from 2010 to 2022. These two stations are located in the north part of the GoC, 13 km away from each other (Figure 2a). As explained in the previous section, the $\delta v/v_s$ were computed with a sliding window of 60 days in the 1–3 s period band. Assuming that coda waves are dominated by surface waves, in the 1–3 s period band, their depth sensitivity is maximum at shallow depth of the order of 1–2 km (Yang et al., 2019).

At both stations, we observe relative change of velocity of the order of $\pm 0.1\%$. However, the temporal evolution of the velocity is clearly different at both sites. At MALA, the evolution of the seismic velocity is dominated by a seasonal pattern, the velocity being larger during the winter and lower during the summer. By contrast, at AGRP no clear seasonal variation of the seismic wave velocity is observed.

This example indicates that $\delta v/v$ measurements can vary spatially over distances of the order of 10 km and that in some specific locations the measurements are dominated by seasonal variations.

3. Seasonal Variations of the Seismic Velocities in Greece

We have seen in the previous section that at station CL.MALA located in the GoC, the temporal evolution of the seismic velocity measured on coda waves in the 1–3 s period band is dominated by seasonal variations. In this section, we further attempt to characterize and understand the origin of these seasonal variations at the scale of Greece. We first determine in which regions the evolution of the seismic wave velocity is dominated by seasonal variations.

To that end, we compute the $\delta v/v$ at each station as described in Section 2.3. Following (Wang et al., 2017), we quantify the magnitude of the seasonal variations by calculating a seasonality coefficient. For each seismological station, we compare the annual $\delta v/v$ between 2010 and 2021 by computing a correlation coefficient between the

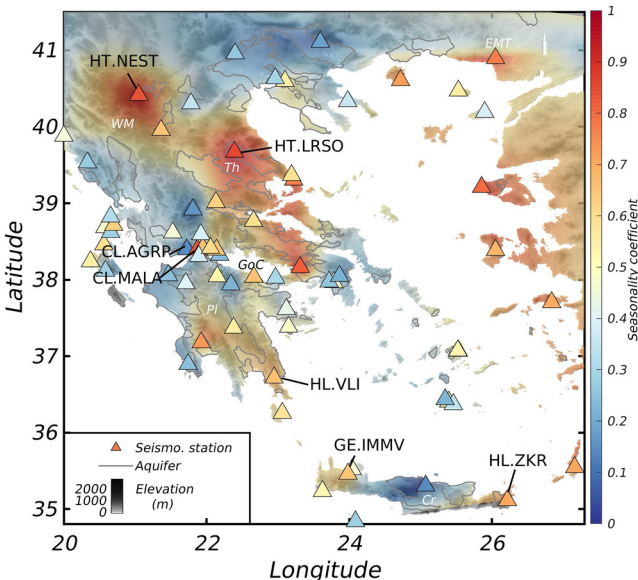


Figure 4. Map of the seasonality coefficient in Greece obtained from $\delta v/v$ measurements computed in the 1–3 s period band. Alluvial and karst aquifers are indicated by solid gray lines (from the work of Margat, 2008). The seasonality coefficient is greater than 0.6 in specific regions indicating that the evolution of seismic wave velocity is dominated by seasonal variations: (a) the northern part of the Gulf of Corinth; (b) the coastal part of the Peloponnese (PI); (c) the southeastern part of Crete (Cr); (d) Thessaly region (Th); (e) East Macedonia and Thrace (EMT) and (f) western Macedonia(WM).

than 0.6, indicating that they exhibit seasonal variations: (a) the northern part of the GoC; (b) the coastal part of the Peloponnese; (c) the southeastern part of Crete; (d) Thessaly region; (e) East Macedonia and Thrace and, (f) western Macedonia (WM). There is a first-order correlation between the regions where $\delta v/v$ vary seasonally and the alluvial and karstic aquifers map from Margat (2008), which is shown in the background of Figure 4.

4. Origin of the Seasonal Variations on the $\delta v/v$ in Greece

Several factors could explain why the seismic wave velocity varies with the season in several regions in Greece, such as seasonal changes in the distribution of the seismic noise sources, the surface temperature, or the groundwater level. However, we do not believe that the two first explanations are relevant. Indeed, if the velocity variations measured on auto-correlations were only apparent changes due to seasonal changes in the distribution of noise sources we would expect them (a) to be similar at nearby stations and (b) to occur simultaneously at all stations. Yet, this is not the case in Greece. As shown in Figure 2, the $\delta v/v$ obtained at nearby stations can vary greatly and the seasonal velocity changes do not occur simultaneously at all concerned stations (Figure 2 and in Text S2 in Supporting Information S1). Thus it is unlikely that our observations can be explained only by the dynamics of the noise sources.

Furthermore, several studies such as (Compaire et al., 2022; Hillers et al., 2015; Richter et al., 2014), have highlighted that temperature changes can affect seismic velocities by inducing thermoelastic strain at shallow depths. In this case, the velocity changes are expected to decay with depth. However, as discussed in Text S3 in Supporting Information S1 we observe that in some regions, the seasonal variations of seismic velocities are larger in the 2–3 s period band than between 1 and 2 s. Assuming that the auto-correlations of coda waves are dominated by surface waves so that their depth sensitivity increases with the period, this rules out the possibility that our observations are explained by thermoelastic strain.

Instead, the primary cause of the seasonal $\delta v/v$ variations observed in Greece is likely to be the annual hydrological cycles (Barajas et al., 2021; Clements & Denolle, 2018; Mao et al., 2022; Poli et al., 2020; Tsai, 2011)

$\delta v/v$ measured each year (Figure 3). We define the seasonality coefficient as an average of all these correlations coefficients:

$$SC = \frac{1}{N} \sum_{i=2010}^{2019} \sum_{j=i+1}^{2020} \frac{\text{cov}(\delta v/v_i, \delta v/v_j)}{\sigma_i \sigma_j} \quad (2)$$

where SC is the seasonality coefficient obtained at a given station for a given period band, σ_i and σ_j are the variances of the $\delta v/v$ measured for the year i and j respectively. A value close to 1 indicates that the $\delta v/v$ calculated each year are similar and thus dominated by seasonal variations. Conversely, low values indicate that the $\delta v/v$ is not dominated by seasonal variations. We consider that $\delta v/v$ measurements are dominated by seasonal variations if SC is greater than 0.6.

An example of measurement done at the station MALA is provided in Figure 3. The upper panel presents the $\delta v/v$ measured from 2014 to 2020 in the 1–3 s period band. The lower panel shows the $\delta v/v$ measured each year superimposed on each other. Each year, the $\delta v/v$ measured at the station MALA in the 1–3 s period band evolve in a similar way, the seismic velocities being lower in August than in January. For this particular station, we obtain a seasonality coefficient of 0.85 which confirms that the evolution of the seismic wave velocity is dominated by variations having a period of 1 year.

We map the $\delta v/v$ seasonality coefficient by interpolating the value obtained at each station using a natural neighbor interpolation. Figure 4 shows the results obtained in the 1–3 s period band. The map indicates that $\delta v/v$ measurements are not dominated by seasonal variations everywhere in Greece. Instead, specific regions are associated with a seasonality coefficient greater

21699356, 2023, 12, Downloaded from https://agupubs.onlinelibrary.wiley.com/doi/10.1029/2023JB026759 by Cachan France, Wiley Online Library on [30/11/2023]. See the Terms and Conditions (https://onlinelibrary.wiley.com/terms-and-conditions) on Wiley Online Library for rules of use; OA articles are governed by the applicable Creative Commons License

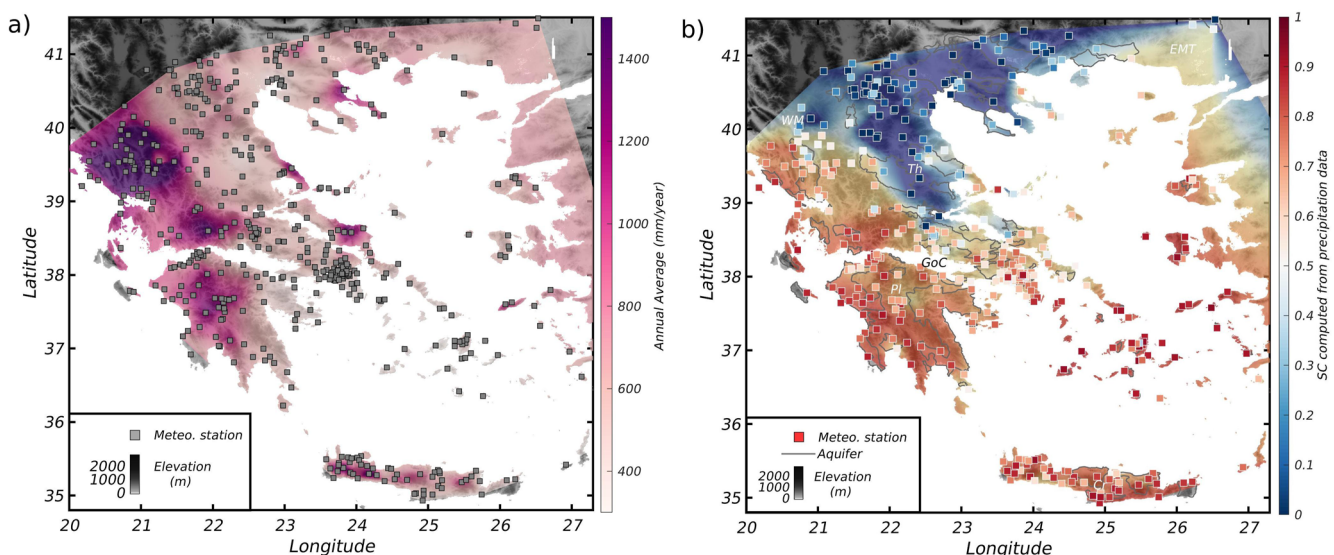


Figure 5. (a) Average rainfall per year in Greece: precipitations are not homogeneous and vary from 400 mm/year in the east to 1,500 mm/year in the west. (b) Seasonality coefficient map for precipitations measured at 494 weather stations (square) between 2010 and 2021. The seasonality coefficient obtained at each station is interpolated spatially using a natural neighbor interpolation. We observe that precipitations exhibit a clear seasonal behavior in the southwest part of Greece but not in the northeast region.

that are related to two main factors: natural rainfall and anthropogenic well pumping that depletes groundwater in summers.

4.1. Monitoring Aquifers Using $\delta v/v$ and GPS Measurements

Silverii et al. (2016) have shown, using GPS data in the Apennines, that the multiyear hydrological cycle associated with the phase of recharge and discharge of karst aquifer causes an extensional deformation of 3 mm/year. The vertical deformation displays seasonal and multiyear variations reflecting the elastic response of the lithosphere to variations in surface water loads. This hydrological forcing associated with the recharge of karst aquifers induces a measurable surface deformation of up to 50 nanostrain per year (D'Agostino, 2014).

Unlike GPS measurements, $\delta v/v$ is an in-situ measurement of the evolution of the mechanical properties of the crust that are affected by variations in pore pressure, porosity, saturation, density, and the presence of micro-cracks. Changes in groundwater level induced by precipitation or anthropogenic well pumping can cause variations in seismic velocities by two main mechanisms: the loading pressure exerted by the water can subside the surface, leading to an elastic response of the subsurface. In addition, by filling the open pore space between soil grains and thus increasing the pore pressure of the subsurface, precipitation induces a poroelastic response that can generate a local rise of the surface. In this case, an increase in the amount of water in the aquifer increases the pore pressure, which reduces the overall effective pressure, and thus the seismic wave velocity (Hillers et al., 2014; Sens-Schönfelder & Wegler, 2006).

The effect of rainfalls and well pumping on seismic velocities depends also on the nature of the considered aquifer. Confined aquifers such as the Las Vegas Basin (Alley et al., 1999) or the Thessaly basin in Greece ("Th" on Figure 4) are bounded by (relatively) impermeable layers. This prevents or delays the vertical flow of groundwater induced by precipitation. Groundwater pumping in confined aquifers made of unconsolidated sediments causes a decrease of water pressure in the reservoir that results in sediment compaction (Alley et al., 1999; Parcharidis et al., 2011; Salvi et al., 2004). This results in faster seismic velocities and a surface subsidence (Bettinelli et al., 2008; Faunt et al., 2016; Galloway et al., 1999; Overacker et al., 2022). By contrast, in unconfined aquifers, a decrease in the amount of groundwater, for instance, induced by anthropological pumping or evapotranspiration, induces a mass discharge that causes an uplift of the surface (Overacker et al., 2022).

4.2. Seasonal Variation of Rainfall in Greece

To assess whether precipitation may be driving the seasonality of velocity variations, we use 12 years of rainfall data collected by 494 weather stations distributed throughout Greece (Figure 1). As shown in Figure 5a, precipitations are not homogeneous in Greece, but vary from 400 mm/year in the east to 1,500 mm/year in the west. We present examples of rainfall records from three stations in Text S4 in Supporting Information S1. Two of them exhibit seasonal variations (Pylos and Ios, located in the South Peloponnese and on the island of Santorini respectively) whereas there is no seasonal variation at the third one which is located in the Thessaly region.

In order to determine in which region the precipitation exhibits an annual cycle, a seasonality coefficient for precipitation is computed in the same way as the $\delta v/v$ measurement (Section 3). We first smooth the precipitation records with a 2-month sliding window that reduces short-term fluctuations and highlights long-term variations. Then, a correlation coefficient is computed between the precipitation recorded each year from 2010 to 2021. For each weather station, the seasonality coefficient is defined as the average of these correlation coefficients.

The precipitation seasonality map is shown in Figure 5b. Two areas can be clearly distinguished: the northeast part of Greece where the seasonality coefficient is lower than 0.3 indicating that precipitation does not vary according to the seasons (WM and Thessaly). On the contrary, in the southwest part of Greece, the seasonality coefficient is greater than 0.8 meaning that the precipitation follows an annual cycle.

Comparing Figures 4 and 5b, it is clear that the seasonality maps of $\delta v/v$ and rainfall are not correlated. North of the GoC, in the western part of Peloponnese, in the central part of Crete the $\delta v/v$ vary with the season, but not the precipitation. However, in the south of the GoC, locally in the Peloponnese and in the Cyclades, precipitation and velocity variations are both seasonal. In these areas, rainfall may be the driving force of the seasonal variations of the seismic velocity.

4.3. Can the Seismic Velocity Seasonal Variations Be Predicted From Precipitations?

In order to evaluate the effect of rain on the velocity of seismic waves, we use a simple linear reservoir model to estimate the water levels in the subsurface following the work of Barajas et al. (2021). We assume that precipitation supplies water in the aquifer through a rapid process but also the aquifer loses water at a rate that is proportional to the water level. Energy is lost during the discharge resulting in an exponential decrease in water level after rainfall events (Barajas et al., 2021; Fiorillo, 2011).

The discharge rate $Q(t)$ as a function of time t is then:

$$Q(t) = \exp(-kt), \quad (3)$$

k is the proportionality coefficient between the rate at which the aquifer loses water and the water level. It is expressed in day⁻¹ and represents the rate at which water flows out of the aquifer.

Moreover, we assume that the aquifer is recharged by precipitation through a rapid process, which is a valid assumption when considering mediums with a high permeability such as karsts or carbonates. Thus, the water level $h(t)$ within the aquifer is expressed as a convolution between the daily precipitation P and the discharge rate Q :

$$h(t) = Q(t) \otimes P(t), \quad (4)$$

where \otimes denotes the convolution operator. In the case where the seismic velocity variations are influenced by the water level inside the aquifer, the velocity and water level variations should be correlated. Assuming a linear relationship between the velocity variations and the water level inside the aquifer, it is possible to predict velocity variations from precipitations similarly to (Rivet et al., 2015):

$$\delta v/v_{syn}(t) = <\delta v/v(t)> + \frac{cov[\delta v/v(t), h(t)]}{\text{var}(h(t))} * h(t) \quad (5)$$

There is a single free parameter k which is determined through a simple grid search by minimizing the misfit between the observed and predicted $\delta v/v$. The misfit function σ that we minimize is defined as:

$$\sigma^2(k) = \frac{1}{n} \sum_{i=1}^n (\delta v/v(i) - \delta v/v_{syn}(i, k))^2 \quad (6)$$

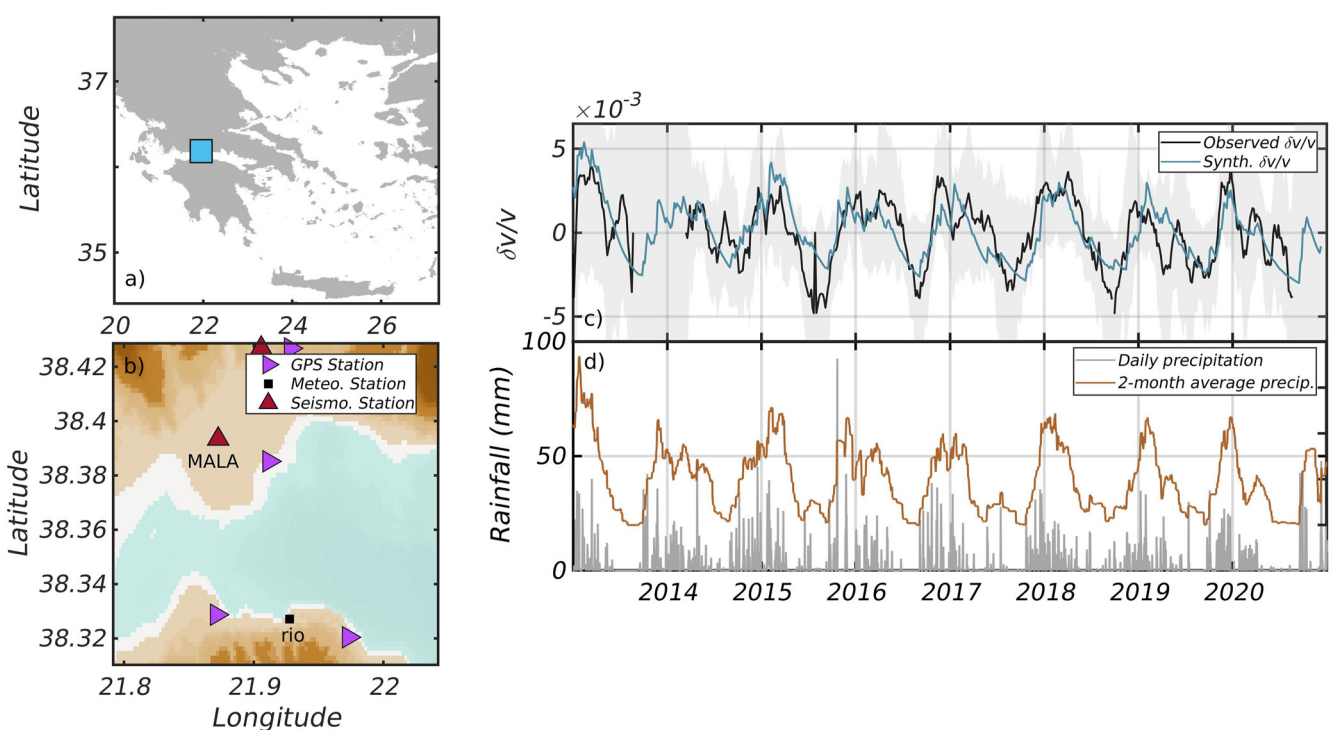


Figure 6. $\delta v/v$ predicted from precipitation at the seismic station MALA. (a) Map of Greece showing the area where the station MALA is located (blue square). (b) Zoom on the region where MALA is located (red triangle). Precipitation data come from the Rio station (black square). (c) Observed $\delta v/v$ in the 2–3 s period band (black line) compared with $\delta v/v$ predicted from precipitation data using a linear reservoir model (blue solid line). (d) Daily precipitation (gray bar) and cumulative precipitation with a 2-month sliding window average (brown solid line).

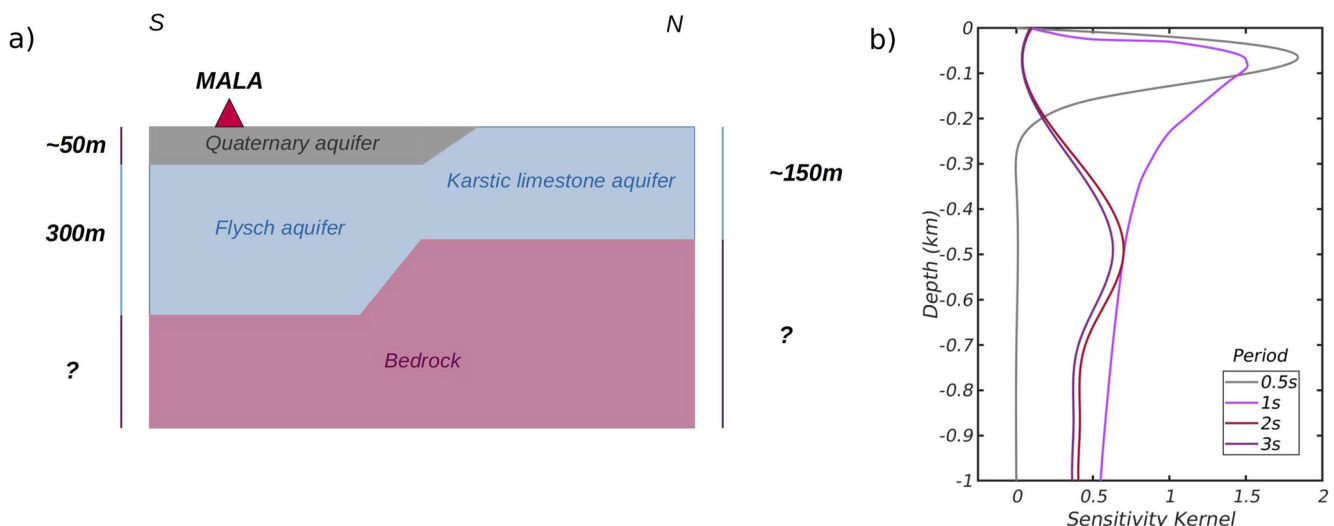


Figure 7. Cross-section of Mornos delta and Rayleigh waves sensitivity kernel at the station MALA. (a) Schematic North-South cross-section of the Mornos delta beneath the station MALA (from the information of Louis et al., 2004; Parcharidis et al., 2013). (b) Sensitivity kernels of Rayleigh waves as a function of depth at periods 0.5, 1, 2, and 3 s computed in the 1D medium shown on the left panel. At 0.5 and 1 s of periods, the sensitivity of the Rayleigh waves is maximum at a depth of 100 m, whereas at 2 and 3 s of periods it is a maximum at 500 m. To compute sensitivity kernels, geological units are converted into seismic velocity assuming that in the 15–55 s lapse time windows, coda waves are dominated by Rayleigh waves (velocities from Zhang et al., 2009).

The chosen synthetic $\delta v/v$ is the one associated with the parameter k which minimizes the difference between the observed and the synthetic $\delta v/v$.

4.3.1. Predicting $\delta v/v$ From Precipitation: An Example Where Seismic Velocities Are Positively Correlated With Precipitation

The MALA seismological station is located in the northwestern GoC, on the Mornos river's delta (Figures 6a and 6b). This delta is made up of alluvium with an average thickness of about 50 m (but could reach 100 m in some places). The underlying layer is a flysch whose lower limit beneath the station reaches 350 m. To the north of the delta, limestones are present. According to the various borehole logs (Parcharidis et al., 2013), limestones and flysch coexist at the same depth with a progressive north-south limestones-flysch gradient (Louis et al., 2004). In these formations, 3 aquifers co-exist: one in the alluvium, one in the flysch, and one in the karst system (Louis et al., 2004) (Figure 7).

Figure 6d, shows the precipitation measured at the weather station Rio located 12 km from the seismological station MALA from 2013 to 2021. The cumulative rainfall obtained with a sliding window of two months presents an annual cycle (Parcharidis et al., 2013): the precipitation being maximum in November–February and minimum in June–August. As shown by Figure 6c, in the 2–3 s period band, the seismic wave velocity varies in the same way as the precipitation: the $\delta v/v$ varies according to the annual cycle having an amplitude of about $\pm 0.3\%$, the velocities being maximum when the precipitations are maximum in November–February.

As explained in the previous section, we compute a synthetic $\delta v/v$ from precipitation for different values of k ranging from 0 to 1, and for each k we compute the misfit between the observed and synthetic $\delta v/v$ (see Text S5 in Supporting Information S1). We present in Figure 6c the synthetic $\delta v/v$ obtained for the value of k which minimizes the misfit.

In this example, the best fit is obtained for $k = 0.0167 \text{ day}^{-1}$ corresponding to a characteristic time of 60 days (Figure 6c). The correlation coefficient between the observed and synthetic $\delta v/v$ is then 0.72 indicating it is possible to predict accurately the observed seismic velocity variation from rainfall records. This is consistent with the fact that the misfit function presents a clear global minimum (see Text S5 in Supporting Information S1). As shown in Figure 6c, both predicted and synthetic $\delta v/v$ exhibit a clear annual cycle having an amplitude of 0.3%, the largest velocities being observed during winter.

Assuming that in the 15–55 s lapse time windows, coda waves are dominated by Rayleigh waves, we can estimate to which depth the $\delta v/v$ measurements are sensitive. To this end, we compute Rayleigh sensitivity kernels at 0.5, 1, 2, and 3 s of period in a 1D layered medium that reflects the local geology (Figure 7). The velocities V_p , V_s and the density of the rocks ρ have been chosen depending of the rock types according to the values obtained by Zhang et al. (2009). In the 2–3 s period band, the sensitivity of Rayleigh waves is maximum at a depth of 500 m that is below the 3 aquifers located beneath MALA. Thus the $\delta v/v$ is positively correlated with the precipitation since the measurements are sensitive to variations of the load pressure exerted by the water within the aquifers.

4.3.2. Predicting $\delta v/v$ From Precipitation: An Example Where Seismic Velocities Are Anti-Correlated With Precipitation

In the previous section, we showed an example of an unconfined shallow alluvial aquifer for which the $\delta v/v$ measurements are sensitive to depths greater than the aquifer. In this case, the seismic velocity variations are related to the elastic response of the medium to variations in the amount of water. They are thus positively correlated with precipitation.

In this section, we discuss the velocity variations at the station IMMV located in western Crete. This station is located on carbonate rocks of the Trypolis series (thickness of 400 m) within which a karstic aquifer of high permeability is located (Kanta et al., 2009, 2013; Parisi et al., 2013).

On Figure 8, we compare the GPS and precipitation records with the $\delta v/v$ computed in the 1–2 s period band. Measurements performed in the 0.5–1 s and 2–3 s period bands are shown in Text S3 in Supporting Information S1. In the 0.5–1 s similar seasonal variations are observed but with higher amplitudes than 1–2 s. On the other hand, no seasonal behavior is visible at higher periods.

The $\delta v/v$ observed in the 1–2 s period band exhibits seasonal variations having an amplitude of $\approx 0.2\%$ (Figure 8c). They are anti-correlated with precipitation: the $\delta v/v$ are sensitive to depths similar to the aquifer so that the seismic velocity decreases when the amount of water within the aquifer increases. The observed $\delta v/v$ and the

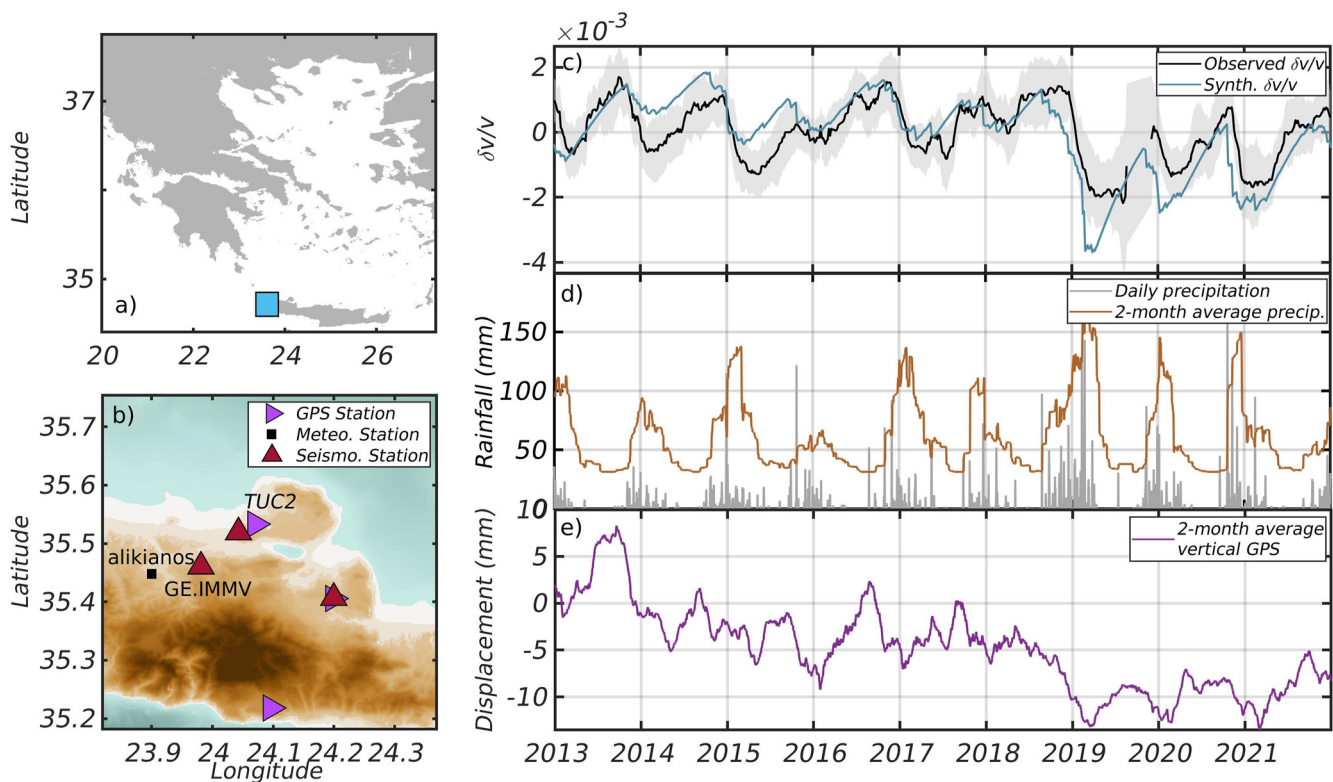


Figure 8. Velocity variations measured at the IMMV station that is located over an unconfined karstic aquifer. (a) Map of Greece showing the area where the IMMV seismological station is located (blue rectangle). (b) Zoom on the region where the IMMV seismic station (red triangle), the TUC2 GPS station (purple triangle) and the Alikianos weather stations (black square) are located. (c) Observed $\delta v/v$ in the 1–2 s period band (black solid line) and $\delta v/v$ predicted from precipitation using a linear reservoir model (blue solid line). (d) Daily precipitation (gray bar) and cumulative precipitation obtained with a 2-month sliding window (brown solid line). (e) 2-month averaged vertical displacement measured at the GPS station TUC2 located 11 km away from the seismic station IMMV.

synthetic $\delta v/v$ computed from precipitation using a linear reservoir model have a correlation coefficient of 0.75, indicating that it is possible to predict the velocity variations from rainfall.

We compare the velocity variations with the vertical displacement of the surface recorded by a GPS station located 12 km away from IMMV (Figure 8e). The vertical displacement shows a long-term subsidence of the surface that is not correlated with a long-term change in seismic velocity. In addition to this long-term trend, the vertical displacement exhibits seasonal changes whose amplitude varies from year to year. These seasonal fluctuations are anti-correlated with precipitations: there is an uplift each summer when precipitation is minimum and vice-versa in winter. This indicates that the aquifer beneath IMMV is unconfined.

4.3.3. Generalization to All Sites and Characteristic Time of Aquifers Assuming a Linear Reservoir Model

As we have seen in previous sections, in specific regions of Greece, the hydrological cycle induces seasonal changes in seismic wave velocity (Figure 4). Following the procedure described in Section 4.3, for each station where the seismic wave velocity varies with the season, we try to predict the observed $\delta v/v$ from the precipitation recorded at the nearest meteorological station using a simple linear reservoir model. As shown in Figure 9, we found that for 18 sites, the absolute value of the correlation coefficient between observed and predicted $\delta v/v$ between 2012 and 2021 is greater than 0.57 (table in Text S6 in Supporting Information S1).

We observe that there are two main types of sites. At 11 stations, the seasonal change in velocity is positively correlated with the water level predicted from precipitation (purple squares in Figure 9). All of these stations are located over shallow alluvial aquifers. Therefore, the change in seismic velocity measured between 1 and 3 s is sensitive to the elastic response of the subsurface induced by the dynamic of the aquifer. We find that at most of these sites, the characteristic time τ varies between 35 and 60 days, with the exception of two sites where we find

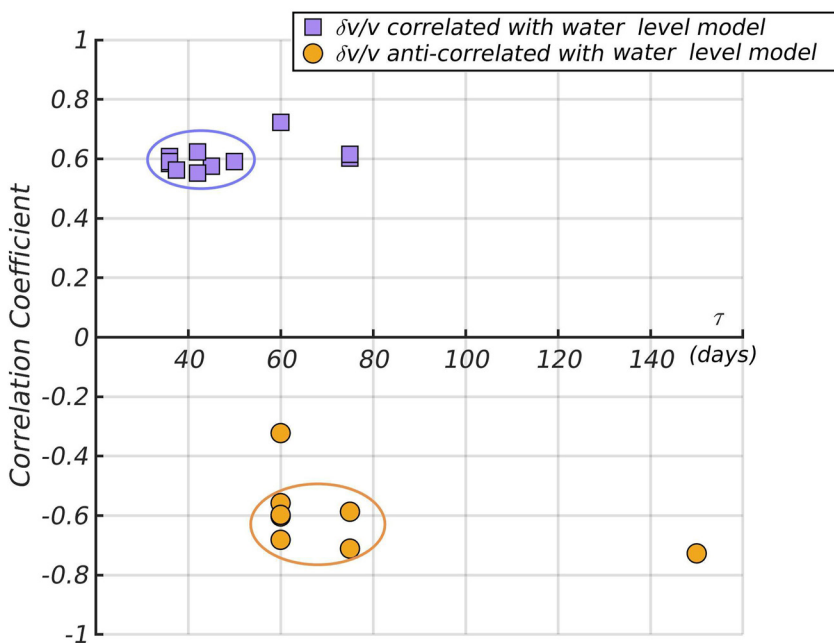


Figure 9. Correlation coefficient between observed $\delta v/v$ and predicted $\delta v/v$ from precipitation as a function of the characteristic time $\tau = 1/k$. Stations for which $\delta v/v$ are positively and negatively correlated with water level inside the aquifer are shown respectively with blue squares and orange circles.

a characteristic time τ of 75 days: HL.VLI which is located in southeast Peloponnese over metamorphic rocks and CL.MG05 located north of the GoC over alluvial deposits.

In contrast, at nine stations, the seasonal change in velocity is anti-correlated with the water level predicted from precipitation (orange circles in Figure 9). These stations are likely located over deep karstic aquifers so that the seismic velocities between 1 and 3 s are mostly sensitive to the poroelastic response induced by the hydrologic cycle, the velocity decreasing as the amount of water within the aquifers increases. We find a characteristic time τ ranging from 60 to 80 days for these sites, with the exception of the IMMV station for which the characteristic time τ is equal to 150 days.

Finally, monitoring the temporal variation of seismic velocities is a promising tool, which can be used together with other geophysical observations to identify the dynamic of aquifers and others processes in the crust. In particular, $\delta v/v$ measured on seismic noise auto-correlations allows the detection of periodic variations of the groundwater level, to distinguish between deep and shallow aquifers while giving an indication of the discharge rate of the aquifer. The deployment of dense networks could allow a to study the dynamics of aquifers with a greater temporal and spatial resolution and become a useful tool for water supply management.

4.4. Seismic Velocities Variations Associated With Water Pumping

In the Mediterranean basin, aquifers are the main exploitable resource for drinking water supply and agricultural exploitation. The increase in population and tourism, the concentration of agricultural and industrial practices, the decrease in precipitation, and the increase in evapotranspiration due to climate change in recent decades, lead to excessive exploitation of groundwater resources (Aureli et al., 2008). This affects particularly coastal aquifers which are sensitive areas. Indeed, excessive pumping in these regions induces a decrease in the fluid pressure inside the aquifer, that can lead to seawater intrusion. When this occurs, the interface between seawater and freshwater intrusion progresses landward until a new equilibrium is reached (Daskalaki & Voudouris, 2008; Ergil, 2000; Voudouris et al., 2004).

In some inland areas, the extent of groundwater extraction, especially for irrigation needed for agriculture, exceeds the rate of aquifer recharge. This is the case of Thessaly (Central Greece) which is one of the most active regions

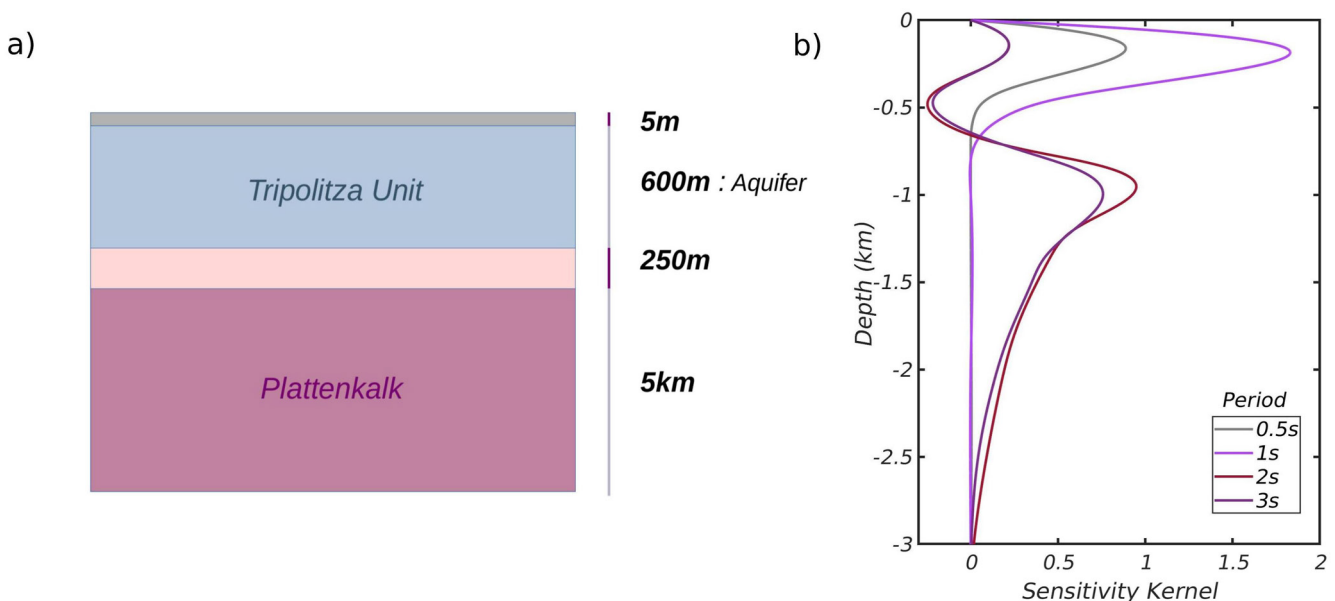


Figure 10. Sensitivity kernel and cross-section computed at Zakros region. (a) Schematic cross-section of the rocks below the ZKR seismological station. The gray layer represents the superficial layer of limestone, below the carbonate flysch sandstones where the aquifer is located. The light pink color represents the impermeable layer composed of carbonate and volcanic rocks. Finally, the Plattenkalk unit is composed of limestone, carbonate marls, and shales metabauxite (informations from Kavouri & Karatzas, 2015; Papanikolaou & Vassilakis, 2010; Ring & Yngwe, 2018). (b) Sensitivity kernel showing that the maximum of the sensitivity is at the level of the aquifer in the 0.5–1 s (250 m) while for higher periods (2–3 s), the sensitivity is maximal at 1 km depth: below the aquifer system.

in terms of agricultural exploitation (Daskalaki & Voudouris, 2008). The over-exploitation leads to a condensation of the sediments at depth which results in a depletion at the surface. This can create fractures and weakens buildings.

Thus, monitoring aquifers has become essential from a societal but and ecological point of view. The long-term evolution of $\delta v/v$ could potentially be used as an indicator of the evolution of water resources on a multi-year scale, which is particularly relevant in water-stressed countries like Greece.

In the previous section, we have shown that for most seismic stations located on aquifers, it is possible to deduce the variations in seismic wave velocity related to the hydrological cycle from the precipitation using a simple linear reservoir model. However, at specific sites, the hydrologic cycle is also strongly influenced by anthropogenic pumping, so it is not possible to predict seismic wave velocity variations from precipitation.

Here, we specifically study how water pumping for agriculture and industry induces seismic wave velocity changes at two seismic stations ZKR and LRSO which are located over an unconfined and a confined aquifer respectively. The long-term goal would be to use $\delta v/v$ measurements to study the evolution of the water resource on a large scale, in addition to hydraulic heads and surface deformation measurements.

4.4.1. Seismic Waves Velocity Variations Associated With Water Pumping in an Unconfined Aquifer

The study area is a carbonate plateau of 132 km², located in eastern Crete. More precisely, the plateau consists of shallow Neogene superficial deposits (sandstones, marly limestones and conglomerates) extending over the 600 m thick limestone and dolomite series (Figure 10b). This carbonate series, which contains the aquifer, overlies the impermeable volcano-sedimentary sequence of the “Phyllite—Tyros bed” (Kavouri et al., 2016; Papanikolaou & Vassilakis, 2010). In this area, water is pumped mainly for irrigation during the dry period that is from April to November (Kavouri & Karatzas, 2015; Papanikolaou & Vassilakis, 2010).

Since the local geology is known from previous studies (Kavouri et al., 2016; Papanikolaou & Vassilakis, 2010), we can convert the geological unit into seismic velocity assuming that the early coda is dominated by surface waves. This makes it possible to assess the depth sensitivity of $\delta v/v$ measurements done in several period bands. As shown by Figure 10, the sensitivity of Rayleigh waves is maximum at a depth of about 200 m at 0.5–1 s, and at a depth of 1 km at 2–3 s of period.

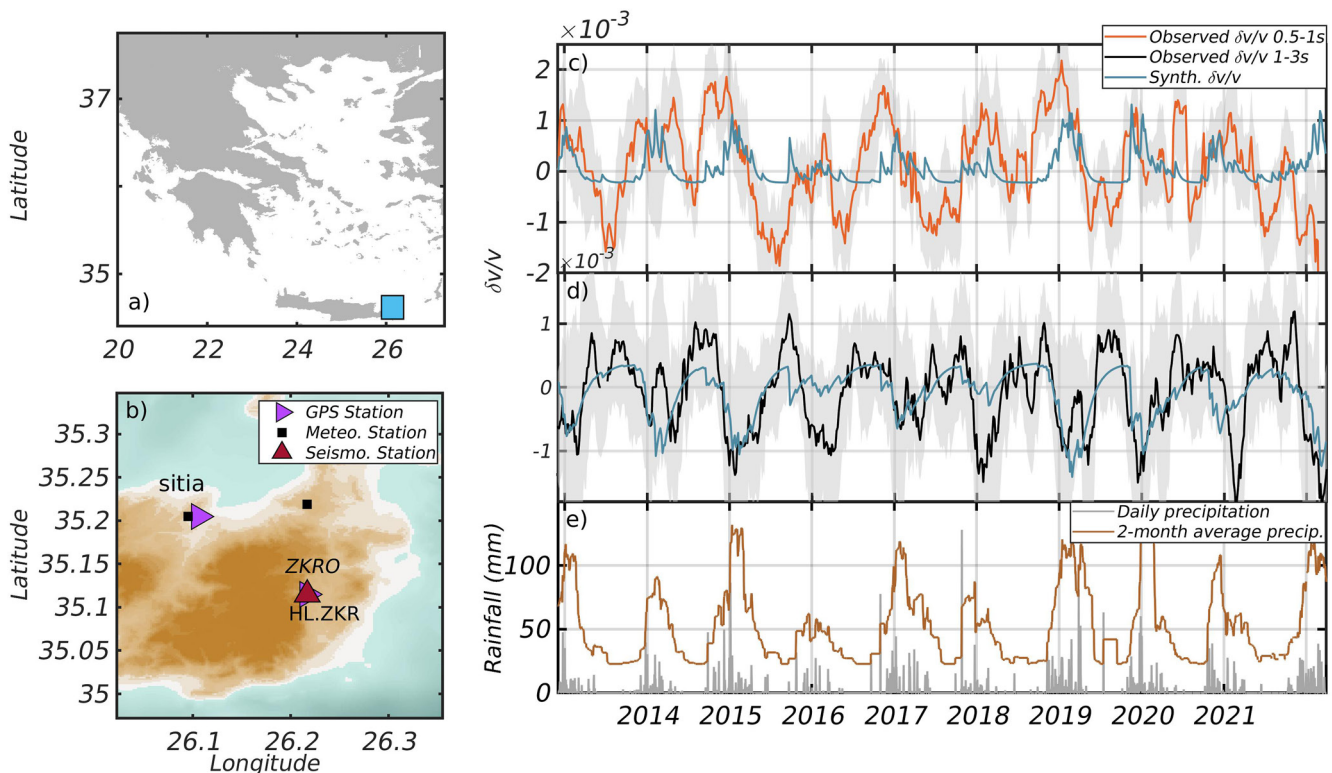


Figure 11. Seismic velocity variation at the station ZKR which is located over an unconfined karst aquifer used for water pumping. (a) Map of Greece showing the area where the seismic station ZKR is located (blue rectangle). (b) Zoom on the region where the ZKR seismic station (red triangle) and the weather station sitia (black square) are located. (c) Observed $\delta v/v$ in the 0.5–1 s period band (orange solid line) compared with $\delta v/v$ predicted from precipitation records using a linear reservoir model (blue solid line). (d) Observed $\delta v/v$ in the 1–3 s period band (black solid line) compared with $\delta v/v$ predicted from precipitation (blue solid line). (e) Daily precipitation (gray bar) and cumulative precipitation obtained with a 2-month sliding window (brown solid line).

Figure 11 shows the $\delta v/v$ measurements in the 0.5–1 s and 1–3 s period obtained with a sliding window of 60 days. In both period bands, the seismic velocity exhibits seasonal variations, but they have a different phase and amplitude. Between 0.5 and 1 s, Rayleigh waves are sensitive to the uppermost 500 m where the aquifer lies. Seismic velocity increases progressively during the dry season when water is pumped and are maximum at the beginning of the winter when the ground water level is minimum (Figure 11e). The seasonal variation in seismic velocity has an amplitude of 0.2%. At longer periods, between 1 and 3 s, Rayleigh waves are mainly sensitive to depth ranging from 700 to 1,500 m, that is they see the medium below the aquifer. In this period band, the seasonal variations have an amplitude of only 0.1%, the maximum velocity being in winter and the minimum in summer. This is the opposite than between 0.5 and 1 s, since in this period band the $\delta v/v$ measurement is sensitive to the elastic response of the crust to the change in groundwater level.

The synthetic $\delta v/v$ have been computed in both periods using the precipitations data from Sitia meteorologic station located 16 km away from seismological station ZKR (Figures 11c–11e). The aim is to determine if precipitations can be the driven mechanism at the origin of the seasonal behavior exhibited by the velocity variations. Thus, in the 0.5–1 s, it is not possible to predict the observed $\delta v/v$ from the precipitation (correlation coefficient = 0.28) (Figure 11c). However, in the 1–3 s of period, the correlation coefficient reaches the value of 0.68 (Figure 11d). These results indicate that seismic velocities record different processes in these two period bands: in 1–3 s of period, an elastic effect occurs linked with the filling of the aquifer by precipitation while in the 0.5–1 s, the pumping effect is predominant.

4.4.2. Seismic Waves Velocity Variations Due To Water Pumping in a Confined Aquifer

To study the effects of water pumping in a confined aquifer on seismic wave velocity, we focus on the station HT.LRSO which is located in Thessaly (Figure 12). This region includes two distinct large alluvial aquifer systems: the western unconfined aquifers that extend along the Trikala and Karditsa plains, and the eastern

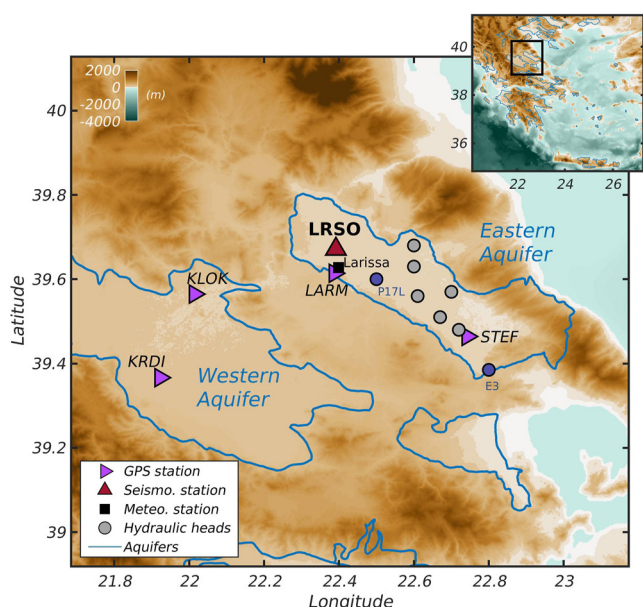


Figure 12. Map of Thessaly showing the location of two main alluvial aquifers: the western aquifer located within the Trikala and Karditsa plain; and the eastern aquifer where the LRSO station (red triangle) is located. GPS stations are indicated by magenta triangles, and boreholes used to monitor the water level from 1997 to 2013 by gray circles. The two blue circles represent the two boreholes analyzed in this study.

being recharged laterally during the rainy season (November–March) when the water is not used for agriculture (Argyarakis et al., 2020; Seferli et al., 2019). In addition, all the measurements of groundwater levels exhibit a negative long-term trend indicating the progressive depletion of the aquifer. Between 1997 and 2012, the water level dropped by approximately 20 m in the northern part of the aquifer against 45 m in the southern part (Figure 13) (Sidiropoulos et al., 2016).

This annual cycle is controlled by the precipitation that recharges laterally the aquifers, and the pumping of water that takes place every year during the dry season (April–October) to support agriculture and the cultivation of cotton (Aureli et al., 2008; Sidiropoulos et al., 2016). The long term trend from 1997 to 2012 is due to the excessive pumping of water that leads a depletion of water resources and to a compaction of sediments within the aquifer which in turn leads to significant soil subsidence especially in summer and autumn when the groundwater pumping is at maximum (Foumelis et al., 2016; Parcharidis et al., 2011; Salvi et al., 2004; Sidiropoulos et al., 2016; Vassilopoulou et al., 2013).

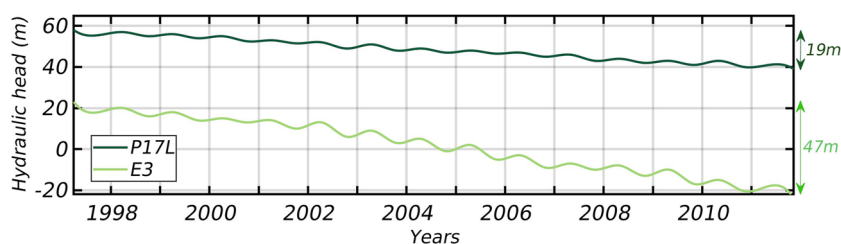


Figure 13. Hydraulic heads recorded at P17L and E3 wells in Western Thessaly. The two time series presents annual variations of amplitude 2 and 5 m respectively and a long-term trend. Between 1997 and 2012, the water level dropped by approximately 20 m in the borehole P17L located at the northern part of the aquifer against 45 m in the southern part (E3) (Information from Sidiropoulos et al., 2016).

confined aquifers that in the Larissa and Karla plains (Argyarakis et al., 2020). In both aquifer system, pumping for agriculture occurs using wells (Foumelis et al., 2016; Ilia et al., 2016; Parcharidis et al., 2011; Rozos et al., 2010; Salvi et al., 2004; Seferli et al., 2019).

Here, we analyze the seismic velocity variations within the eastern confined aquifer using the seismological station LRSO (Figure 12). The studies of Caputo et al. (1994), Caputo and Pavlides (1993), and Konstantinides (1978) indicates that in this area the basement rocks can reach a depth of 500–700 m in some locations. Quaternary sediments overlie the basement rocks, primarily composed of carbonate rocks, and shales. Multiple alternations of coarse-grained permeable deposits (aquifers) with impermeable to low-permeability strata (aquitards) create a number of successive semi-confined to confined aquifers (Argyarakis et al., 2020; Kontogianni et al., 2007). The majority of these aquifers, however, seem to be rather isolated from each others, which prevents in most cases their recovery after intense exploitation (Kontogianni et al., 2007).

4.4.2.1. Hydraulic Heads Seasonal Variations and Long-Term Trend

Precipitation in this area does not exhibit clear seasonal fluctuations but still remains rare from June to August (Figure 14d) and reaches annual average of 700 mm (Figure 5a).

The groundwater level in the eastern alluvial aquifers has been monitored using boreholes placed along the aquifer from 1997 to 2012 (Figures 12 and 13). At all boreholes, the groundwater level exhibits seasonal variations having an amplitude ranging from 2 to 5 m, the groundwater level being maximum in May/April and minimum in October/November, the aquifers

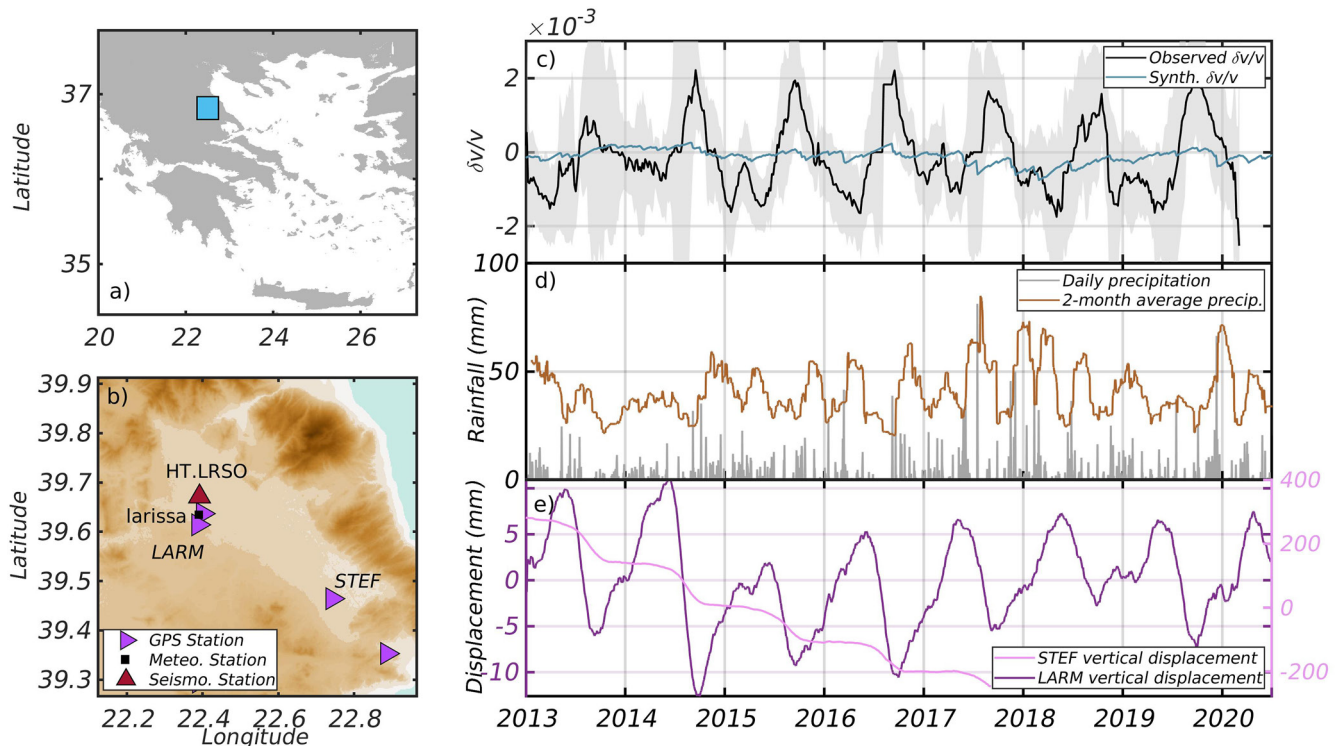


Figure 14. Seismic velocity variation at the station LRSO which is located over a confined alluvial aquifer used for water pumping. (a) Map of Greece indicating the area where seismic station LRSO is located (blue square). (b) Zoom on the region where the LRSO seismic station (red triangle), the LARM and STEF GPS stations (purple triangle) and the weather station Larissa (black square) are located. (c) Observed $\delta v/v$ in the 1–3 s period band (black solid line) compared with the $\delta v/v$ predicted from precipitation records using a linear reservoir model (blue solid line). (d) Daily precipitation (gray bar) and cumulative precipitation obtained with a 2-month sliding window. (e) Vertical displacement measured at the GPS station LARM and STEF located respectively at 6 and 37 km from LRSO averaged with a two 2-month sliding window.

4.4.2.2. Seismic Velocity Variations in a Confined Aquifer

As shown by Figure 14c, between 1 and 3 s, the seismic velocity measured at LRSO exhibits a clear seasonal fluctuations with an amplitude of $\pm 0.2\%$, the velocity being maximum in October and minimum in April. The correlation coefficient computed between the synthetic $\delta v/v$ predicted from precipitation and the observed one is equal to 0.23. This low value indicates that the observed $\delta v/v$ cannot be predicted from precipitation.

We compare the velocity changes with the hydraulic head measurements even though the two time series do not overlap (the $\delta v/v$ are measured from 2013 to 2020 and the hydraulic head from 1997 to 2012). Assuming that the seasonal changes in hydraulic head are similar in 2013–2020 and 1998–2012, we find that the decrease in hydraulic head of 2 m occurring each year from May to October at borehole P17L corresponds to an increase in $\delta v/v$ of 0.2%. Thus, at this site, the $\delta v/v$ are anti-correlated with changes in hydraulic head and appear to be exceptionally sensitive to changes in the water level. Mao et al. (2022) showed that $\delta v/v$ measurements are more sensitive to water-level changes in confined aquifers than in unconfined aquifers. In the Los Angeles and Santa Ana basins, which are confined aquifers, they reported that water table level changes of 1 m are associated with a $\delta v/v$ of 0.01%. By contrast we find that $\delta v/v$ is 10 times more sensitive to ground water level changes.

4.4.2.3. Vertical Displacement and Seismic Velocity Variation

The 2-month averaged vertical displacements measured at the GPS station LARM and STEF that is located north and south of the East Thessaly aquifer, 6.4 and 37.9 km away from the seismic station LRSO respectively, is shown in Figure 14e. Similarly to the $\delta v/v$, the vertical displacements at LARM exhibit a seasonal behavior with an uplift of 15 mm in March/April when the seismic wave velocity is minimal and the groundwater level is maximum. Despite the fact that the time series between hydraulic heads measurements and GPS/ $\delta v/v$ don't overlap, we suppose that the behavior of the hydraulic heads remain the same during the period 2013–2020. Thus, we can quantify the vertical movement of the GPS (at LARM station) with the water level within the aquifer and

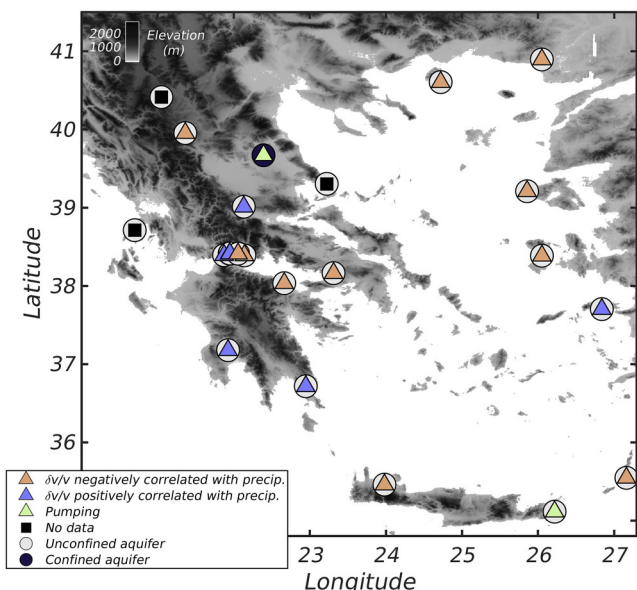


Figure 15. Map showing the location of the poro-elastic and elastic effect seen by the velocity variations in the 1–3 s period band. Seismic stations for which $\delta v/v$ exhibits seasonal variations that are positively and negatively correlated with precipitations are shown with blue and orange triangles respectively. Seismic stations for which $\delta v/v$ cannot be predicted from precipitations and are likely due to water pumping are shown in green. We distinguish stations in the vicinity of confined and unconfined aquifers (black and white circle surrounding the stations).

ally at a single aquifer or to changes in water level induced by sediment compaction at depth. This illustrates that GPS, hydraulic head and $\delta v/v$ measurements are complementary to each other.

5. Conclusion

In the Mediterranean basin, aquifers are the main exploitable resource for drinking water supply and agricultural exploitation. The increasing demands of the last decades attend to excessive exploitation of groundwater resources. This can leads either to the depletion of aquifers, or to their contamination by seawater intrusion. Thus, monitoring these resources has become crucial. Greece is currently ranked 26th (Heggie, 2020) in the world among the countries most affected by water stress.

Currently, in Greece, agriculture represents the main demand for water and covers about 86% of the total water consumption (Daskalaki & Voudouris, 2008). There are two types of aquifers in Greece: karst aquifers, which are mainly found in carbonate rocks and cover about 35% of the country; and aquifers located in alluvial layers dating from the Neogene and Quaternary periods.

The aim of this study was to investigate the extent to which seismic noise auto-correlations can be useful for monitoring the long-term evolution of water resources at the scale of a country. By investigating how seismic velocities are affected by the hydrological cycle in Greece, it highlights the possibility of using seismic noise correlations to detect periodic depth variations of the amount of water within aquifers due to precipitation or anthropic activities. By probing the medium at depth, the information provided by noise correlations coda waves is a complement to GPS/INSAR surface observation and hydraulic head measurements.

Specifically, we measure the temporal evolution of the seismic velocity at all public broadband stations in Greece between 2010 and 2022, using seismic noise auto-correlations in the 1–3 s period band. At specific sites and regions, the $\delta v/v$ shows clear seismic variations with amplitude on the order of 0.1% (Figure 4). These sites are all located over or near aquifers, suggesting that the annual variation in seismic velocities is related to slow strain perturbation associated with the hydrological cycle.

the velocity variations in a case of a confined aquifer. An increase of 0.2% of the $\delta v/v$ corresponds to a drop of the vertical displacement of 15 mm and approximately to a drop in groundwater level of 2 m.

As pointed out by Argyrakis et al. (2020), the comparison between the two GPS LARM and STEF indicates different long-term trends. A negative trend is clearly visible at STEF located to the southeast of the aquifer (Figure 14d). The vertical displacement registers an annual variation like at LARM station: a decrease occurs in summer during pumping. However, from October to July a “flat” trend is visible. This annual characteristic indicates that the aquifer fails to regenerate during the wet season. Furthermore, a negative long-term trend is also visible: the vertical displacement between 2013 and 2017 decreases by about 0.5 m (Figure 14d, light pink). This negative trend cannot be explained by precipitation, which has remained constant in recent years. This is probably a consequence of the progressive water level depletion in the aquifer (Figure 13) associated with deep sediment consolidation occurring in the area is the cause of this marked decrease on the GPS.

In summary, the $\delta v/v$, GPS, and hydraulic head measurements do not provide the same information on the dynamic of the aquifer system. The hydraulic head and GPS measurements exhibit both seasonal fluctuations and a long-term trend that may be the consequence of sediment consolidation at depth (Foumelis et al., 2016; Parcharidis et al., 2011; Salvi et al., 2004; Sidiropoulos et al., 2016; Vassilopoulou et al., 2013) and the progressive aquifer depletion. Despite seasonal variations in hydraulic head, vertical displacement of the surface and $\delta v/v$ are well correlated, no long-term variation in $\delta v/v$ is observed. One possible explanation is that, since $\delta v/v$ is an in-situ and volumetric measurement, it is primarily sensitive to the amount of water stored in the entire aquifer system and not to changes in water level measured punctually at a single aquifer or to changes in water level induced by sediment compaction at depth. This illustrates that GPS, hydraulic head and $\delta v/v$ measurements are complementary to each other.

Taking advantage of the dense network of weather stations in Greece, and using a linear reservoir model, we show that at 12 sites, the observed $\delta v/v$ can be predicted from precipitation (Figure 15). For deep karstic aquifers, the velocity change follows the hydrological cycle with a velocity drop for increasing hydraulic head and vice versa. This is in agreement with previous studies (e.g., Barajas et al., 2021; Hillers et al., 2015; Poli et al., 2020; Wang et al., 2017). However, as shown in Figure 15, we found that for shallow alluvial aquifers, the 1–3 s auto-correlations coda waves are sensitive to a depth greater than the aquifer itself, so that the $\delta v/v$ are positively correlated with the amount of water within the aquifer: the seismic velocities are minimum when the amount of water is minimum. For both types of aquifers, we found that the seasonal velocity changes are correlated with the vertical motion of deformation: these seasonal changes are associated to a transient deformation of the crust occurring in response to the variation of the hydraulic head in the aquifer. Predicting the observed $\delta v/v$ variations from precipitation using a linear reservoir model, allow to estimate the characteristic time of the discharge rate of the aquifer. We find a characteristic time ranging from 35 to 50 days for most of the alluvial aquifers and from 60 to 75 days for karstic systems.

In some regions such as Thessaly and in Crete, water is used intensively during the dry season for agriculture, the hydrological cycle is strongly influenced by anthropogenic pumping. Hence we found that the seasonal velocity change cannot be predicted from precipitation. However, they are clearly correlated with fluctuations in groundwater levels measured in boreholes.

Finally, we show that the effects of water pumping are different for confined and unconfined aquifers. As shown in Figure 11, pumping water from an unconfined aquifer causes a decrease of the loading pressure that is associated with an uplift of the surface (Bettinelli et al., 2008; Faunt et al., 2016; Galloway et al., 1999; Overacker et al., 2022), and a relaxation at depth that results in a decrease in seismic velocity. On other hand, pumping water in a confined aquifer results in sediment compaction within the aquifer and is associated with a subsidence of the surface and a decrease in seismic velocity (Figure 14). From the hydraulic heads measurement obtained by Sidiropoulos et al. (2016), we can quantify approximately in Thessaly region the velocity variations in terms of water level fluctuations for a confined aquifer: thus, an increase of 0.2% of the $\delta v/v$ corresponds approximately to a drop of groundwater level of 2 m and a drop of the vertical displacement of 15 mm.

Data Availability Statement

The sensitivity kernels have been computed using the Python library disba that implements a subset of codes from Computer Programs in Seismology (Herrmann, 2013). The Vp, Vs of the rocks has been chosen according to the study of Luu (2021) and Zhang et al. (2009).

Waveform data used in this paper belong to the networks with codes: CL, Corinth Rift Laboratory Team and RESIF Datacenter (2013), GE, GEOFON Data Centre (1993), HA, University of Athens (2008), HC, Technological Educational Institute of Crete (2006), HL, National Observatory of Athens, Institute of Geodynamics, Athens (1975), HP, University of Patras (2000), HT, Aristotle University of Thessaloniki (1981), KO, Kandilli Observatory and Earthquake Research Institute, Boğaziçi University (1971). The data set can be retrieved on the International Federation of Digital Seismograph Networks website (FDSN, <https://www.fdsn.org/networks/>).

The meteorological data are provided by the Institute of Environmental Research and Sustainable Development (IERSD) and the National Observatory of Athens (NOA). The 495 stations used in this study are available on the website Meteo.gr (stratus.meteo.noa.gr/front). We gather the GPS displacements from 210 permanent stations from rinex data of the Nevada Geodetic Laboratory (NGL) (Blewitt et al., 2018). These data were processed using the Jet Propulsion Laboratory GIPSY-OASIS II software following the procedure used in Metois et al. (2015) (geodesy.unr.edu/NGLStationPages/stations/).

The velocity variations measurements presented in this article are archived at Zenodo (Delouche, 2023) and can be downloaded from Github (github.com/EstelleDelouche).

Acknowledgments

This article has been supported by the project “Real-time earthquake risk reduction for a reSilent Europe” (RISE), funded by the European Union’s Horizon 2020 research and innovation program under Grant Agreement Number 821115.

References

- Alley, W. M., Reilly, T. E., & Franke, O. L. (1999). *Sustainability of ground-water resources* (Vol. 1186). US Department of the Interior, US Geological Survey.
Almagro Vidal, C., Zaccarelli, L., Pintori, F., Bragato, P. L., & Serpelloni, E. (2021). Hydrological effects on seismic-noise monitoring in karstic media. *Geophysical Research Letters*, 48(15), e2021GL093191. <https://doi.org/10.1029/2021GL093191>

- Amoruso, A., Crescentini, L., Martino, S., Petitta, M., & Tallini, M. (2014). Correlation between groundwater flow and deformation in the fractured carbonate Gran Sasso aquifer (INFN underground laboratories, central Italy). *Water Resources Research*, 50(6), 4858–4876. <https://doi.org/10.1002/2013wr014491>
- Amos, C. B., Audet, P., Hammond, W. C., Bürgmann, R., Johanson, I. A., & Blewitt, G. (2014). Uplift and seismicity driven by groundwater depletion in central California. *Nature*, 509(7501), 483–486. <https://doi.org/10.1038/nature13275>
- Argus, D. F., Fu, Y., & Landerer, F. W. (2014). Seasonal variation in total water storage in California inferred from GPS observations of vertical land motion. *Geophysical Research Letters*, 41(6), 1971–1980. <https://doi.org/10.1002/2014gl059570>
- Argyraakis, P., Ganas, A., Valkaniotis, S., Tsionumas, V., Sagias, N., & Psihogios, B. (2020). Anthropogenically induced subsidence in Thessaly, central Greece: New evidence from GNSS data. *Natural Hazards*, 102(1), 179–200. <https://doi.org/10.1007/s11069-020-03917-w>
- Aristotle University of Thessaloniki. (1981). Aristotle university of Thessaloniki seismological network [Dataset]. International Federation of Digital Seismograph Networks. <https://doi.org/10.7914/SN/HT>
- Aureli, A., Ganoulis, J., & Margat, J. (2008). Groundwater resources in the Mediterranean region: Importance, uses and sharing. *Water in the Mediterranean*, 96–105.
- Barajas, A., Poli, P., d'Agostino, N., Margerin, L., & Campillo, M. (2021). Separation of poroelastic and elastic processes of an aquifer from tectonic phenomena using geodetic, seismic, and meteorological data in the Pollino Region, Italy. *Geochemistry, Geophysics, Geosystems*, 22(11), e2021GC009742. <https://doi.org/10.1029/2021gc009742>
- Bawden, G. W., Thatcher, W., Stein, R. S., Hudnut, K. W., & Peltzer, G. (2001). Tectonic contraction across Los Angeles after removal of groundwater pumping effects. *Nature*, 412(6849), 812–815. <https://doi.org/10.1038/35090558>
- Bettinelli, P., Avouac, J.-P., Flouzat, M., Bollinger, L., Ramillien, G., Rajaura, S., & Sapkota, S. (2008). Seasonal variations of seismicity and geodetic strain in the Himalaya induced by surface hydrology. *Earth and Planetary Science Letters*, 266(3–4), 332–344. <https://doi.org/10.1016/j.epsl.2007.11.021>
- Blewitt, G., Hammond, W., & Kreemer, C. (2018). Harnessing the GPS data explosion for interdisciplinary science. *Eos*, 99. <https://doi.org/10.1029/2018eo104623>
- Borsa, A. A., Agnew, D. C., & Cayan, D. R. (2014). Ongoing drought-induced uplift in the western United States. *Science*, 345(6204), 1587–1590. <https://doi.org/10.1126/science.1260279>
- Brenguier, F., Campillo, M., Hadzioannou, C., Shapiro, N. M., Nadeau, R. M., & Larose, É. (2008). Postseismic relaxation along the San Andreas Fault at Parkfield from continuous seismological observations. *Science*, 321(5895), 1478–1481. <https://doi.org/10.1126/science.1160943>
- Brenguier, F., Clarke, D., Aoki, Y., Shapiro, N. M., Campillo, M., & Ferrazzini, V. (2011). Monitoring volcanoes using seismic noise correlations. *Comptes Rendus Geoscience*, 343(8–9), 633–638. <https://doi.org/10.1016/j.crte.2010.12.010>
- Caputo, R., Bravard, J.-P., & Helly, B. (1994). The Pliocene-quaternary tecto-sedimentary evolution of the Larissa plain (eastern Thessaly, Greece). *Geodinamica Acta*, 7(4), 219–231. <https://doi.org/10.1080/09853111.1994.11105267>
- Caputo, R., & Pavlides, S. (1993). Late Cainozoic geodynamic evolution of Thessaly and surroundings (central-northern Greece). *Tectonophysics*, 223(3–4), 339–362. [https://doi.org/10.1016/0040-1951\(93\)90144-9](https://doi.org/10.1016/0040-1951(93)90144-9)
- Chaussard, E., Bürgmann, R., Shirzaei, M., Fielding, E. J., & Baker, B. (2014). Predictability of hydraulic head changes and characterization of aquifer-system and fault properties from InSAR-derived ground deformation. *Journal of Geophysical Research: Solid Earth*, 119(8), 6572–6590. <https://doi.org/10.1002/2014jb011266>
- Chen, B., & Liu, Z. (2016). Global water vapor variability and trend from the latest 36 year (1979 to 2014) data of ECMWF and NCEP reanalyses, radiosonde, GPS, and microwave satellite. *Journal of Geophysical Research: Atmospheres*, 121(19), 11–442. <https://doi.org/10.1002/2016jd024917>
- Clements, T., & Denolle, M. A. (2018). Tracking groundwater levels using the ambient seismic field. *Geophysical Research Letters*, 45(13), 6459–6465. <https://doi.org/10.1029/2018gl077706>
- Compaire, N., Margerin, L., Monnereau, M., Garcia, R. F., Lange, L., Calvet, M., et al. (2022). Seasonal variations of subsurface seismic velocities monitored by the SEIS-insight seismometer on mars. *Geophysical Journal International*, 229(2), 776–799. <https://doi.org/10.1093/gji/gjab499>
- Corinth Rift Laboratory Team and RESIF Datacenter. (2013). CL - Corinth Rift Laboratory Seismological Network (CRLNET) [Dataset]. RESIF - Réseau Sismologique et géodésique Français. <https://doi.org/10.15778/resif.cl>
- D'Agostino, N. (2014). Complete seismic release of tectonic strain and earthquake recurrence in the Apennines (Italy). *Geophysical Research Letters*, 41(4), 1155–1162. <https://doi.org/10.1002/2014gl059230>
- Daskalaki, P., & Voudouris, K. (2008). Groundwater quality of porous aquifers in Greece: A synoptic review. *Environmental Geology*, 54(3), 505–513. <https://doi.org/10.1007/s00254-007-0843-2>
- Delouche, E. (2023). Velocity variations in Greece and seasonality coefficient [Software]. <https://doi.org/10.5281/zenodo.8387634>
- Ergil, M. E. (2000). The salination problem of the Guzelyurt aquifer, Cyprus. *Water Research*, 34(4), 1201–1214. [https://doi.org/10.1016/s0043-1354\(99\)00253-5](https://doi.org/10.1016/s0043-1354(99)00253-5)
- Faunt, C. C., Sneed, M., Traum, J., & Brandt, J. T. (2016). Water availability and land subsidence in the central valley, California, USA. *Hydrogeology Journal*, 24(3), 675–684. <https://doi.org/10.1007/s10040-015-1339-x>
- Fiorillo, F. (2011). Tank-reservoir drainage as a simulation of the recession limb of karst spring hydrographs. *Hydrogeology Journal*, 19(5), 1009–1019. <https://doi.org/10.1007/s10040-011-0737-y>
- Foumelis, M., Papageorgiou, E., & Stamatopoulos, C. (2016). Episodic ground deformation signals in Thessaly plain (Greece) revealed by data mining of SAR interferometry time series. *International Journal of Remote Sensing*, 37(16), 3696–3711. <https://doi.org/10.1080/01431161.2016.1201233>
- Frappart, F., & Ramillien, G. (2018). Monitoring groundwater storage changes using the gravity recovery and climate experiment (GRACE) satellite mission: A review. *Remote Sensing*, 10(6), 829. <https://doi.org/10.3390/rs10060829>
- Froment, B., Campillo, M., Chen, J., & Liu, Q. (2013). Deformation at depth associated with the 12 May 2008 M_w 7.9 Wenchuan earthquake from seismic ambient noise monitoring. *Geophysical Research Letters*, 40(1), 78–82. <https://doi.org/10.1029/2012gl053995>
- Froment, B., Campillo, M., Roux, P., Gouédard, P., Verdel, A., & Weaver, R. L. (2010). Estimation of the effect of nonisotropically distributed energy on the apparent arrival time in correlations. *Geophysics*, 75(5), SA85–SA93. <https://doi.org/10.1190/1.3483102>
- Galloway, D. L., & Burbey, T. J. (2011). Regional land subsidence accompanying groundwater extraction. *Hydrogeology Journal*, 19(8), 1459–1486. <https://doi.org/10.1007/s10040-011-0775-5>
- Galloway, D. L., Jones, D. R., & Ingebritsen, S. E. (1999). *Land subsidence in the United States* (Vol. 1182). US Geological Survey.
- GEOFON Data Centre. (1993). GEOFON seismic network [Dataset]. Deutsches GeoForschungsZentrum GFZ. <https://doi.org/10.14470/TR560404>
- Hadzioannou, C., Larose, E., Baig, A., Roux, P., & Campillo, M. (2011). Improving temporal resolution in ambient noise monitoring of seismic wave speed. *Journal of Geophysical Research*, 116(B7), B07304. <https://doi.org/10.1029/2011jb008200>

- Heggie, J. (2020). Preventing a water crisis in Greece, National Geographic. Retrieved from <https://www.nationalgeographic.com/science/article/partner-content-where-our-water-goes-greece>
- Herrmann, R. B. (2013). Computer programs in seismology: An evolving tool for instruction and research. *Seismological Research Letters*, 84(6), 1081–1088. <https://doi.org/10.1785/0220110096>
- Hillers, G., Ben-Zion, Y., Campillo, M., & Zgone, D. (2015). Seasonal variations of seismic velocities in the San Jacinto fault area observed with ambient seismic noise. *Geophysical Journal International*, 202(2), 920–932. <https://doi.org/10.1093/gji/ggv151>
- Hillers, G., Campillo, M., Brenguier, F., Moreau, L., Agnew, D., & Ben-Zion, Y. (2019). Seismic velocity change patterns along the San Jacinto fault zone following the 2010 $M_{7.2}$ El Mayor-Cucapah and $M_{5.4}$ Collins valley earthquakes. *Journal of Geophysical Research: Solid Earth*, 124(7), 7171–7192. <https://doi.org/10.1029/2018jb017143>
- Hillers, G., Campillo, M., & Ma, K.-F. (2014). Seismic velocity variations at TCDP are controlled by MJO driven precipitation pattern and high fluid discharge properties. *Earth and Planetary Science Letters*, 391, 121–127. <https://doi.org/10.1016/j.epsl.2014.01.040>
- Ilia, I., Loupasakis, C., & Tsangaratos, P. (2016). Assessing ground subsidence phenomena with persistent scatterer interferometry data in western Thessaly, Greece. *Bulletin of the Geological Society of Greece*, 50(3), 1693–1702. <https://doi.org/10.12681/bgsg.11892>
- Ji, K. H., & Herring, T. A. (2012). Correlation between changes in groundwater levels and surface deformation from GPS measurements in the San Gabriel Valley, California. *Geophysical Research Letters*, 39(1), L01301. <https://doi.org/10.1029/2011gl050195>
- Kandilli Observatory and Earthquake Research Institute, Boğaziçi University. (1971). Kandilli observatory and earthquake research institute (KOERI) [Dataset]. International Federation of Digital Seismograph Networks. <https://doi.org/10.7914/SN/KO>
- Kanta, A., Soupios, P., Barsukov, P., Kouli, M., & Vallianatos, F. (2013). Aquifer characterization using shallow geophysics in the Keritis Basin of western Crete, Greece. *Environmental Earth Sciences*, 70(5), 2153–2165. <https://doi.org/10.1007/s12665-013-2503-z>
- Kanta, A., Soupios, P., Vallianatos, F., Rust, D., & Barsukov, P. (2009). The application of time domain electromagnetic method to characterize the Keritis Basin, in western Crete, Greece. In *Proceeding of the 3rd IASME/WSEAS international conference on geology and seismology*.
- Kavouri, K., & Karatzas, G. (2015). Spatially distributed recharge in karst groundwater modelling. In *9th World congress of EWRA*.
- Kavouri, K., Karatzas, G., & Moraetis, D. (2016). Evaluation of temporal storage zones in karstic aquifers using hydrogeochemical analysis. In *2nd EWaS international conference, Chania, Crete, Greece, 1–4 June 2016. Theme H: Groundwater and irrigation systems, ID 137*.
- King, N., Argus, D., Langbein, J., Agnew, D., Bawden, G., Dollar, R., et al. (2007). Space geodetic observation of expansion of the San Gabriel Valley, California, aquifer system, during heavy rainfall in winter 2004–2005. *Journal of Geophysical Research*, 112(B3), B03409. <https://doi.org/10.1029/2006jb004448>
- Konstantinides, D. (1978). Hydrodynamique d'un système aquifère hétérogène (Doctorat these).
- Kontogianni, V., Pytharouli, S., & Stiros, S. (2007). Ground subsidence, quaternary faults and vulnerability of utilities and transportation networks in Thessaly, Greece. *Environmental Geology*, 52(6), 1085–1095. <https://doi.org/10.1007/s00254-006-0548-y>
- Ktenidou, O., & Evangelidis, C. (2023). Seismic monitoring and analysis - Catalogues. Retrieved from <https://www.gein.noa.gr/en/services-products/earthquake-catalogs/>
- Lnari, R., Lundgren, P., Manzo, M., & Casu, F. (2004). Satellite radar interferometry time series analysis of surface deformation for Los Angeles, California. *Geophysical Research Letters*, 31(23), L23613. <https://doi.org/10.1029/2004gl021294>
- Lobkis, O. I., & Weaver, R. L. (2003). Coda-wave interferometry in finite solids: Recovery of p-to-s conversion rates in an elastodynamic billiard. *Physical Review Letters*, 90(25), 254302. <https://doi.org/10.1103/physrevlett.90.254302>
- Louis, I. F., Karantonis, G. A., Voulgaris, N. S., & Louis, F. I. (2004). The contribution of geophysical methods in the determination of aquifer parameters: The case of Mornos River Delta, Greece. *Research Journal of Chemistry and Environment*, 8(4), 41–49.
- Luu, K. (2021). disba: Numba-accelerated computation of surface wave dispersion [Software]. <https://doi.org/10.5281/zenodo.5775195>
- Mao, S., Lecointre, A., van der Hilst, R. D., & Campillo, M. (2022). Space-time monitoring of groundwater fluctuations with passive seismic interferometry. *Nature Communications*, 13(1), 1–9.
- Margat, J. (2008). L'eau des méditerranéens: Situation et perspectives. In *L'eau des Méditerranéens* (pp. 1–288).
- Meier, U., Shapiro, N. M., & Brenguier, F. (2010). Detecting seasonal variations in seismic velocities within Los Angeles basin from correlations of ambient seismic noise. *Geophysical Journal International*, 181(2), 985–996. <https://doi.org/10.1111/j.1365-246x.2010.04550.x>
- Metois, M., D'Agostino, N., Avallone, A., Chamot-Rooke, N., Rabaute, A., Duni, L., et al. (2015). Insights on continental collisional processes from GPS data: Dynamics of the peri-adriatic belts. *Journal of Geophysical Research: Solid Earth*, 120(12), 8701–8719. <https://doi.org/10.1002/2015jb012023>
- Mimikou, M. (2005). Water resources in Greece: Present and future. *Global NEST Journal*, 7(3), 313–322.
- National Observatory of Athens, Institute of Geodynamics, Athens. (1975). National observatory of Athens seismic network [Dataset]. International Federation of Digital Seismograph Networks. <https://doi.org/10.7914/SN/HL>
- Nouibat, A., Stehly, L., Paul, A., Schwartz, S., Bodin, T., Dumont, T., et al. (2022). Lithospheric transdimensional ambient-noise tomography of W-Europe: Implications for crustal-scale geometry of the W-Alps. *Geophysical Journal International*, 229(2), 862–879. <https://doi.org/10.1093/gji/ggab520>
- Obermann, A., Froment, B., Campillo, M., Larose, E., Planès, T., Valette, B., et al. (2014). Seismic noise correlations to image structural and mechanical changes associated with the mw 7.9 2008 Wenchuan earthquake. *Journal of Geophysical Research: Solid Earth*, 119(4), 3155–3168. <https://doi.org/10.1002/2013jb010932>
- Obermann, A., Planès, T., Larose, E., & Campillo, M. (2013). Imaging preeruptive and coeruptive structural and mechanical changes of a volcano with ambient seismic noise. *Journal of Geophysical Research: Solid Earth*, 118(12), 6285–6294. <https://doi.org/10.1002/2013jb010399>
- Ojha, C., Werth, S., & Shirzaei, M. (2019). Groundwater loss and aquifer system compaction in San Joaquin valley during 2012–2015 drought. *Journal of Geophysical Research: Solid Earth*, 124(3), 3127–3143. <https://doi.org/10.1029/2018jb016083>
- Overacker, J., Hammond, W. C., Blewitt, G., & Kreemer, C. (2022). Vertical land motion of the high plains aquifer region of the United States: Effect of aquifer confinement style, climate variability, and anthropogenic activity. *Water Resources Research*, 58(6), e2021WR031635. <https://doi.org/10.1029/2021wr031635>
- Papanikolaou, D., & Vassilakis, E. (2010). Thrust faults and extensional detachment faults in Cretan tectono-stratigraphy: Implications for middle Miocene extension. *Tectonophysics*, 488(1–4), 233–247. <https://doi.org/10.1016/j.tecto.2009.06.024>
- Parcharidis, I., Foumelis, M., & Katsafados, P. (2011). Seasonal ground deformation monitoring over southern Larissa plain (central Greece) by SAR interferometry. In *Advances in the research of aquatic environment* (pp. 497–504). Springer.
- Parcharidis, I., Kourkouli, P., Karymbalis, E., Foumelis, M., & Karathanassi, V. (2013). Time series synthetic aperture radar interferometry for ground deformation monitoring over a small scale tectonically active deltaic environment (Mornos, central Greece). *Journal of Coastal Research*, 29(2), 325–338.
- Parisi, S., Pascale, S., Sdao, F., & Soupios, P. (2013). Assessment and mapping of the intrinsic vulnerability to pollution: An example from Keritis River Basin (northwestern Crete, Greece). *Environmental Earth Sciences*, 70(6), 2659–2670. <https://doi.org/10.1007/s12665-013-2321-3>

- Poli, P., Marguin, V., Wang, Q., d'Agostino, N., & Johnson, P. (2020). Seasonal and coseismic velocity variation in the region of L'Aquila from single station measurements and implications for crustal rheology. *Journal of Geophysical Research: Solid Earth*, 125(7), e2019JB019316. <https://doi.org/10.1029/2019jb019316>
- Richter, T., Sens-Schönfelder, C., Kind, R., & Asch, G. (2014). Comprehensive observation and modeling of earthquake and temperature-related seismic velocity changes in northern Chile with passive image interferometry. *Journal of Geophysical Research: Solid Earth*, 119(6), 4747–4765. <https://doi.org/10.1002/2013jb010695>
- Riel, B., Simons, M., Ponti, D., Agram, P., & Jolivet, R. (2018). Quantifying ground deformation in the Los Angeles and Santa Ana coastal basins due to groundwater withdrawal. *Water Resources Research*, 54(5), 3557–3582. <https://doi.org/10.1029/2017wr021978>
- Ring, U., & Yngwe, F. (2018). "To be, or not to be, that is the question"—The Cretan extensional detachment, Greece. *Tectonics*, 37(9), 3069–3084. <https://doi.org/10.1029/2018tc005179>
- Rivet, D., Brenguier, F., & Cappa, F. (2015). Improved detection of preeruptive seismic velocity drops at the Piton de La Fournaise volcano. *Geophysical Research Letters*, 42(15), 6332–6339. <https://doi.org/10.1002/2015gl064835>
- Rivet, D., Brenguier, F., Shapiro, N., Clarke, D., Peltier, A., & Campillo, M. (2013). Insights on the long-term activity of Piton de La Fournaise volcano from noise-based seismic velocity changes measurements. In *AGU fall meeting abstracts* (Vol. 2013, p. V34B–06).
- Rivet, D., Campillo, M., Shapiro, N. M., Cruz-Atienza, V., Radiguet, M., Cotte, N., & Kostoglodov, V. (2011). Seismic evidence of nonlinear crustal deformation during a large slow slip event in Mexico. *Geophysical Research Letters*, 38(8), L08308. <https://doi.org/10.1029/2011gl047151>
- Rodell, M., Velicogna, I., & Famiglietti, J. S. (2009). Satellite-based estimates of groundwater depletion in India. *Nature*, 460(7258), 999–1002. <https://doi.org/10.1038/nature08238>
- Rozos, D., Sideri, D., Loupasakis, C., & Apostolidis, E. (2010). Land subsidence due to excessive groundwater withdrawal. A case study from Stavros—Farsala site, west Thessaly, Patras Greece. In *12th international congress. Greece, Bulletin of the Geological Society of Greece*.
- Salvi, S., Ganias, A., Stramondo, S., Atzori, S., Tolomei, C., Pepe, A., et al. (2004). Monitoring long-term ground deformation by SAR interferometry: Examples from the Abruzzi, central Italy, and Thessaly, Greece. In *5th International symposium on eastern Mediterranean geology, Thessaloniki, Greece* (pp. 1–4).
- Seferli, S., Modis, K., & Adam, K. (2019). Interpretation of groundwater hydrographs in the west Thessaly basin, Greece, using principal component analysis. *Environmental Earth Sciences*, 78(8), 1–12. <https://doi.org/10.1007/s12665-019-8262-8>
- Sens-Schönfelder, C., & Wegler, U. (2006). Passive image interferometry and seasonal variations of seismic velocities at Merapi volcano, Indonesia. *Geophysical Research Letters*, 33(21), L21302. <https://doi.org/10.1029/2006gl027797>
- Sidiropoulos, P., Mylopoulos, N., & Loukas, A. (2016). Reservoir-aquifer combined optimization for groundwater restoration: The case of Lake Karla watershed, Greece. *Water Utility Journal*, 12, 17–26.
- Silver, P. G., Daley, T. M., Niu, F., & Majer, E. L. (2007). Active source monitoring of cross-well seismic travel time for stress-induced changes. *Bulletin of the Seismological Society of America*, 97(1B), 281–293. <https://doi.org/10.1785/0120060120>
- Silverii, F., d'Agostino, N., Métois, M., Fiorillo, F., & Ventafredda, G. (2016). Transient deformation of karst aquifers due to seasonal and multiyear groundwater variations observed by GPS in southern Apennines (Italy). *Journal of Geophysical Research: Solid Earth*, 121(11), 8315–8337. <https://doi.org/10.1002/2016jb013361>
- Soergel, D., Pedersen, H., Stehly, L., Margerin, L., Paul, A., & Group, A. W. (2020). Coda-Q in the 2.5–20 s period band from seismic noise: Application to the greater Alpine area. *Geophysical Journal International*, 220(1), 202–217. <https://doi.org/10.1093/gji/ggj443>
- Technological Educational Institute of Crete. (2006). Seismological network of Crete [Dataset]. International Federation of Digital Seismograph Networks. <https://doi.org/10.7914/SN/HC>
- Tsai, V. C. (2011). A model for seasonal changes in GPS positions and seismic wave speeds due to thermoelastic and hydrologic variations. *Journal of Geophysical Research*, 116(B4), B04404. <https://doi.org/10.1029/2010jb008156>
- University of Athens. (2008). Hellenic seismological network, University of Athens, Seismological Laboratory [Dataset]. International Federation of Digital Seismograph Networks. <https://doi.org/10.7914/SN/HA>
- University of Patras. (2000). University of Patras, Seismological Laboratory [Dataset]. International Federation of Digital Seismograph Networks. <https://doi.org/10.7914/SN/HP>
- Vassilopoulou, S., Sakkas, V., Wegmuller, U., & Capes, R. (2013). Long term and seasonal ground deformation monitoring of Larissa plain (central Greece) by persistent scattering interferometry. *Open Geosciences*, 5(1), 61–76. <https://doi.org/10.2478/s13533-012-0115-x>
- Voudouris, K., Mandilaras, D., & Antonakos, A. (2004). Methods to define the areal distribution of the salt intrusion: Examples from south Greece. In *Groundwater and saline intrusion, 18th SWIM (Salt Water Intrusion Meeting)*, Cartagena, Spain (no. 15, p. 465).
- Wang, Q.-Y., Brenguier, F., Campillo, M., Lecointre, A., Takeda, T., & Aoki, Y. (2017). Seasonal crustal seismic velocity changes throughout Japan. *Journal of Geophysical Research: Solid Earth*, 122(10), 7987–8002. <https://doi.org/10.1002/2017jb014307>
- Wang, Q.-Y., Campillo, M., Brenguier, F., Lecointre, A., Takeda, T., & Hashima, A. (2019). Evidence of changes of seismic properties in the entire crust beneath Japan after the M_w 9.0, 2011 Tohoku-Oki earthquake. *Journal of Geophysical Research: Solid Earth*, 124(8), 8924–8941. <https://doi.org/10.1029/2019jb017803>
- Weaver, R. L., Hadzioannou, C., Larose, E., & Campillo, M. (2011). On the precision of noise correlation interferometry. *Geophysical Journal International*, 185(3), 1384–1392. <https://doi.org/10.1111/j.1365-246x.2011.05015.x>
- Wegler, U., & Sens-Schönfelder, C. (2007). Fault zone monitoring with passive image interferometry. *Geophysical Journal International*, 168(3), 1029–1033. <https://doi.org/10.1111/j.1365-246x.2006.03284.x>
- Yang, C., Li, G., Niu, F., & Ben-Zion, Y. (2019). Significant effects of shallow seismic and stress properties on phase velocities of Rayleigh waves up to 20 s. *Pure and Applied Geophysics*, 176(3), 1255–1267. <https://doi.org/10.1007/s00024-018-2075-7>
- Zaccarelli, L., Shapiro, N., Faenza, L., Soldati, G., & Michelini, A. (2011). Variations of crustal elastic properties during the 2009 L'Aquila earthquake inferred from cross-correlations of ambient seismic noise. *Geophysical Research Letters*, 38(24), L24304. <https://doi.org/10.1029/2011gl049750>
- Zhang, X., Tsang, L. L., Wang, Y., & Zhao, B. (2009). Petrologic composition model of the upper crust in Bohai Bay Basin, China, based on Lamé impedances. *Applied Geophysics*, 6(4), 327–336. <https://doi.org/10.1007/s11770-009-0039-5>

References From the Supporting Information

- Kallioras, A., & Marinos, P. (2015). Water resources assessment and management of karst aquifer systems in Greece. *Environmental Earth Sciences*, 74(1), 83–100. <https://doi.org/10.1007/s12665-015-4582-5>
- Lappas, I., Sabatakakis, P., & Stefouli, M. (2011). The hydrodynamic behaviour of the coastal karst aquifer system of Zarakas-Parnon (Southeastern Peloponissos). In *Advances in the research of aquatic environment* (pp. 451–458). Springer.
- Pavlides, S., Chatzipetros, A., & Valkaniotis, S. (2008). Active faults of Greece and surroundings. In *Proceedings of the 33rd international geological congress, Oslo, Norway. Abstract*.